# Local time extent of magnetopause reconnection using space-ground coordination

Ying Zou[1,2], Brian M. Walsh[3], Yukitoshi Nishimura[4,5], Vassilis Angelopoulos[6], J. Michael Ruohoniemi[7], Kathryn A. McWilliams[8], Nozomu Nishitani[9]

1. Department of Astronomy and Center for Space Physics, Boston University, Massachusetts, USA
2. Cooperative Programs for the Advancement of Earth System Science, University Corporation for Atmospheric Research, Boulder, Colorado, USA
3. Department of Mechanical Engineering and Center for Space Physics, Boston University, Boston, Massachusetts, USA
4. Department of Electrical and Computer Engineering and Center for Space Sciences, Boston University, Boston, Massachusetts, USA
5. Department of Atmospheric and Oceanic Sciences, University of California, Los Angeles, California, USA
6. Department of Earth, Planetary and Space Sciences, University of California, Los Angeles, California, USA
7. The Bradley Department of Electrical and Computer Engineering, Virginia Tech, Blacksburg, Virginia, USA
8. Institute of Space and Atmospheric Studies, University of Saskatchewan, Saskatoon, Saskatchewan, Canada
9. Center for International Collaborative Research, Institute for Space-Earth Environmental Research, Nagoya University, Nagoya, Japan

Corresponding author: Ying Zou
1. Department of Astronomy and Center for Space Physics, Boston University, Massachusetts, USA
2. Cooperative Programs for the Advancement of Earth System Science, University Corporation for Atmospheric Research, Boulder, Colorado, USA
yingzou@bu.edu

Keyword: 2784 Solar wind–magnetosphere interactions; 2724 Magnetopause, cusp, and boundary layers; 7835 Magnetic reconnection

Abstract

Magnetic reconnection can vary considerably in spatial extents. At the Earth's magnetopause, the extent generally corresponds to the extent in local time. The extent has been probed by multi-spacecraft crossing the magnetopause, but the estimates have large uncertainties because of the assumption of spatially continuous reconnection activity between spacecraft and the lack of information beyond areas of spacecraft coverage. The limitations can be overcome by using radars examining ionospheric flows moving anti-sunward across the open-closed field line boundary. We therefore infer the extents of reconnection using coordinated observations of multi-spacecraft and radars for three conjunction events. We find that when reconnection jets occur at only one spacecraft, only the ionosphere conjugate to this spacecraft shows a channel of fast anti-sunward flow. When reconnection jets occur at two spacecraft and the spacecraft are separated by <1 Re, the ionosphere conjugate to both spacecraft shows a channel of fast anti-sunward flow. The consistency allows us to determine the reconnection jet extent by measuring the ionospheric flows. The full-width-at-half-maximum flow extent is 200, 432, and 1320 km, corresponding to a reconnection jet extent of 2, 4, and 11 Re. Considering that reconnection jets emanate from reconnection of a high reconnection rate, the result indicates that both spatially patchy (a few Re) and spatially continuous and extended reconnection (>10 Re) are possible forms of active reconnection at the magnetopause. Interestingly, the extended reconnection develops from a localized patch via spreading across local time. Potential effects of IMF Bx and By on the reconnection extent are discussed.

## 1. Introduction

A long-standing question in magnetic reconnection is what is the spatial extent of reconnection in the direction normal to the reconnection plane. At the Earth's magnetopause, for a purely southward IMF, this corresponds to the extent in the local time or azimuthal direction. The extent of reconnection has significant relevance to solar wind-magnetosphere coupling, as it controls the amount of energy being passed through the boundary from the solar wind into the magnetosphere and ionosphere. Magnetopause reconnection tends to occur at sites of strictly anti-parallel magnetic fields as anti-parallel reconnection [e.g. *Crooker,* 1979; *Luhmann et al.*, 1984], or occur along a line passing through the subsolar region as component reconnection [e.g. *Sonnerup*, 1974; *Gonzalez and Mozer*, 1974]. Evidence shows either or both can occur at the magnetopause, and the overall reconnection extent can span from a few to 40 Re [*Paschmann et al.*, 1986; *Gosling et al.*, 1990; *Phan and Paschmann*, 1996; *Coleman et al.*, 2001; *Phan et al.*, 2001, 2003; *Chisham et al.*, 2002, 2004, 2008; *Petrinec and Fuselier*, 2003; *Fuselier et al.*, 2002, 2003, 2005, 2010; *Pinnock et al.,* 2003; *Bobra et al.*, 2004; *Trattner et al.*, 2004, 2007, 2008, 2017; *Trenchi et al.,* 2008]. However, reconnection does not occur uniformly across this configuration but has spatial variations [*Pinnock et al.*, 2003; *Chisham et al.*, 2008], and it is the reconnection of high reconnection rates that effectively contributes to the momentum and energy flow within the magnetosphere. Reconnection of high reconnection rates is expected to cause rapid magnetic flux generation and fast reconnection jets. This paper therefore investigates the spatial extent of reconnection through the extents of reconnection jets.

Numerical models show that reconnection tends to occur at magnetic separators, i.e. at the junction between regions of different magnetic field topologies, and global MHD models have identified a spatially continuous separator along the magnetopause [*Dorelli et al.*, 2007; *Laitinen et al.*, 2006, 2007; *Haynes and Parnell*, 2010; *Komar et al.*, 2013; *Glocer et al.*, 2016]. However, little is known about where and over what range along the separators reconnection proceeds at a high rate. Reconnection in numerical simulations can be activated by introducing perturbations of the magnetic field or can grow spontaneously with instability or resistivity inherent in the system [e.g. *Hesse et al.*, 2001; *Scholer et al.*, 2003]. When reconnection develops as patches (as due to the instabilities or localized perturbations), the patches can spread in the direction out of the reconnection plane [*Huba and Rudakov*, 2002; *Shay et al.* 2003; *Lapenta et al.*, 2006; *Nakamura et al.*, 2012; *Shepherd and Cassak*, 2012; *Jain et al.*, 2013]. The patches either remain patchy after spreading if the current layer is thick, or form an extended X-line if the current layer is already thin [*Shay et al.*, 2003].

Studies have attempted to constrain the extent of reconnection based on fortuitous satellite conjunctions where the satellites detect reconnection jets at the magnetopause at different local times nearly simultaneously [*Phan et al.*, 2000, 2006; *Walsh et al.*, 2014a, 2014b, 2017]. The satellites were separated by a few Re in *Phan et al.* [2000] and *Walsh et al.* [2014a, 2014b, 2017], and >10 Re in *Phan et al.* [2006], and this is interpreted as the reconnection being active over a few Re and even 10 Re, respectively. At the magnetopause, reconnection of a few Re is often referred to as spatially patchy [e.g., *Fear et al.*, 2008, 2010], and reconnection of >10 Re is spatially extended [*Dunlop et al.*, 2011; *Hasegawa et al.*, 2016]. The term patchy has also been used to describe the temporal characteristics of reconnection [e.g. *Newell and Meng*, 1991]. But this paper primarily focuses on the spatial properties. The extent has been alternatively determined by studying the structures of newly reconnected flux tubes, i.e., flux transfer events (FTEs) [*Russell* *and Elphic*, 1978; *Haerendel et al.*, 1978]. Conceptual models regard FTEs either as azimuthally narrow flux tubes that intersect the magnetopause through nearly circular holes, as formed by spatially patchy reconnection [*Russell and Elphic*, 1978], or as azimuthally elongated bulge structures or flux ropes that extend along the magnetopause, as formed by spatially extended reconnection [*Scholer*, 1988; *Southwood et al.*, 1987; *Lee and Fu*, 1985]. FTEs have been observed to be on the order of a few Re wide in local time [*Fear et al.*, 2008, 2010; *Wang et al.*, 2005, 2007]. FTEs have also been observed across ~20 Re from the subsolar region to the flanks [*Dunlop et al.*, 2011]. But it is unclear whether these FTEs are branches of one extended bulge or flux rope, or multiple narrow tubes formed simultaneously. When the satellites are widely spaced, it is in general questionable whether a reconnection jet/FTE is spatially continuous between the satellites or whether satellites detect the same moving reconnection jet/FTE. Satellites with a small separation may possibly measure the same reconnection jet/FTE, but only provide a lower limit estimate of the extent. A reconnection jet/FTE may also propagate or spread between satellite detection but satellite measurements cannot differentiate the spatial and temporal effects.

This situation can be improved by studying ionospheric signatures of reconnection and FTEs, since their spatial sizes in the ionosphere can be obtained from wide field ground instruments or Low-Earth orbit spacecraft. The ionospheric signatures include poleward moving auroral forms (PMAFs), channels of flows moving anti-sunward across the open-closed field line boundary [e.g., *Southwood*, 1985], and cusp precipitation [*Lockwood and Smith*, 1989, 1994; *Smith et al.*, 1992]. Radar studies have shown that the flows can differ considerably in size, varying from tens of km [*Oksavik et al.*, 2004, 2005], to hundreds of km [*Goertz et al.*, 1985; *Pinnock et al.*, 1993, 1995; *Provan and Yeoman*, 1999; *Thorolfsson et al.*, 2000; *McWilliams et al.*, 2001a, 2001b], and to thousands of km [*Provan et al.*, 1998; *Nishitani et al.*, 1999; *Provan and Yeoman*, 1999]. A similarly broad distribution has been found for PMAFs [e.g. *Sandholt et al.*, 1986, 1990; *Lockwood et al.*, 1989, 1990; *Milan et al.*, 2000, 2016] and the cusp [*Crooker et al.*, 1991; *Newell and Meng*, 1994; *Newell et al.*, 2007]. This range of spatial sizes in the ionosphere approximately corresponds to a range from <1 to >10 Re at the magnetopause. However, care needs to be taken when interpreting the above ionospheric features, since they could also form due to other drivings such as solar wind dynamic pressure pulses [*Lui and Sibeck*, 1991; *Sandholt et al.*, 1994]. An unambiguous proof of their connection to magnetopause reconnection requires simultaneous space-ground coordination [*Elphic et al.*, 1990; *Denig et al.*, 1993; *Neudegg et al.*, 1999, 2000; *Lockwood et al.*. 2001; *Wild et al.*, 2001, 2005, 2007; *McWilliams et al.*, 2004; *Zhang et al.*, 2008].

Therefore a reliable interpretation of reconnection extent has been difficult due to observation limitations. We will address this by comparing the extents probed by multi-spacecraft and radars using space-ground coordination. On one hand, this enables us to investigate whether reconnection spans continuously between satellites, and how wide reconnection extends beyond satellites. On the other hand, this helps to determine whether reconnection is the driver of ionospheric disturbances and whether the in-situ extent is consistent with the ionospheric disturbance extent.

## 2. Methodology

We study the local time extent of reconnection jets as a characteristic extent of reconnection. We use conjugate measurements between the Time History of Events and Macroscale Interactions during Substorms (THEMIS) [*Angelopoulos*, 2008] and Super Dual Auroral Network (SuperDARN) [*Greenwald et al.*, 1995]. We focus on intervals when the IMF in OMNI data remains steadily southward. We require that two of the THEMIS satellites fully cross the magnetopause nearly simultaneously and that the satellite data provide clear evidence for reconnection occurring or not. The full crossings are identified by a reversal of the Bz magnetic field and a change in the ion energy spectra. The requirements of nearly simultaneous crossings and steady IMF conditions help to reduce the spatial-temporal ambiguity by satellite measurements, where the presence/absence of reconnection jets at different local times likely reflects spatial structures of reconnection. Reconnection can still possibly vary between the two satellite crossings, and we use the radar measurements to examine whether the reconnection of interest has continued to exist and maintained its spatial size.

Identification of reconnection jets in the magnetosphere is based on the fluid (MHD) evidence of magnetopause reconnection. Reconnection accelerates plasma bulk flow to Alfvenic speed producing reconnection jets at the magnetopause, and the acceleration should be consistent with the prediction of tangential stress balance across a rotational discontinuity, i.e. Walen relation [*Hudson*, 1970; *Paschmann et al.*, 1979]. The Walen relation is expressed as

$$\Delta V_{predicted} = \pm(1-\alpha_1)^{1/2}(\mu_o\rho_1)^{-1/2}[B_2(1-\alpha_2)/(1-\alpha_1)-B_1] \qquad (1)$$

Where $\Delta V$ is the change in the plasma bulk velocity vector across the discontinuity. $B$ and $\rho$ are the magnetic field vector and plasma mass density. $\mu_0$ is the vacuum permeability. $\alpha = (p_{\parallel} - p_{\perp})\mu_0/B^2$ is the anisotropy factor where $p_{\parallel}$ and $p_{\perp}$ are the plasma pressures parallel and perpendicular to the magnetic field. The magnetic field and plasma moments are obtained from the fluxgate magnetometer (FGM) [*Auster et al.*, 2008] and the ElectroStatic Analyzers (ESA) instrument [*McFadden et al.*, 2008]. The plasma mass density is determined using the ion number density, assuming a mixture of 95% protons and 5% helium. The subscripts 1 and 2 refer to the reference interval in the magnetosheath and to a point within the magnetopause, respectively. The magnetosheath reference interval is a 10-s time period just outside the magnetopause. The point within the magnetopause is taken at the maximum ion velocity change across the magnetopause.

We ensure that the plasma density at this point is >20% of the magnetosheath density to avoid the slow-mode expansion fan [*Phan et al.*, 1996]. We compare the observed ion velocity change with the prediction from the Walen relation. The level of agreement is measured by $\Delta V^* = \Delta V_{obs} \cdot \Delta V_{predicted} / |\Delta V_{predicted}|^2$, following *Paschmann et al.* [1986]. Here $\Delta Vobs$ is the observed ion velocity change. By convention only the velocity changes with $\Delta V^* > 0.5$ are classified as reconnection jets [e.g., *Phan et al.*, 1996; 2013].

To further ensure that reconnection occurs, we examine the kinetic signature of reconnection, which is D-shaped ion distributions at the magnetopause. As magnetosheath ions encounter newly opened magnetic field lines at the magnetopause, they either transmit through the magnetopause entering the magnetosphere or reflect at the boundary. The transmitted ions have a cutoff parallel velocity (i.e. de-Hoffman Teller velocity) below which no ions could enter the magnetosphere. The D-shaped ion distributions are deformed into a crescent shape as ions travel away from the reconnection site [Broll et al. 2017]. We require the satellites to operate in the Fast Survey or Burst mode in which ion distributions are available at 3 s resolution.

We determine reconnection being active if the plasma velocity change across the magnetopause is consistent with the Walen relation with $\Delta V^* >= 0.5$, and if the ions at the magnetopause show a D shape distribution. Reconnection is deemed absent if neither of the two signatures is detected. We require that at least one of the two satellites observe reconnection signatures. Reconnection is regarded as ambiguous if only one of the two signatures is detected, and such reconnection is excluded from our analysis.

We mainly use the three SuperDARN radars located at Rankin Inlet (RKN, geomagnetic 72.6° MLAT, -26.4° MLON), Inuvik (INV, 71.5° MLAT, -85.1° MLON), and Clyde River (CLY, 78.8° MLAT, 18.1° MLON) to measure the ionospheric convection near the dayside cusp. The three radars have overlapping field of views (FOVs), enabling a reliable determination of the 2-d convection velocity. The FOVs cover the ionosphere >75° MLAT, covering the typical location of the cusp under weak and modest solar wind driving conditions [i.e., *Newell et al.*, 1989] and the high occurrence region of reconnection-related ionospheric flows [*Provan and Yeoman*, 1999] with high spatial resolution. Data from Saskatoon (SAS, 60° MLAT, -43.8° MLON) and Prince George (PGR, 59.6° MLAT, -64.3° MLON) radars are also used when data are available. The measurements of these two radars at far range gates can overlap with the cusp. The radar data have a time resolution of 1-2 min. We focus on observations ±3 h MLT from magnetic noon (approximately 1600-2200 UT). The satellite footprints should be mapped close to the radar FOVs under the Tsyganenko (T89) model [*Tsyganenko*, 1989]. Footprints mapped using different Tsyganenko (e.g., T96 or T01 [*Tsyganenko*, 1995, 2002a, 2002b]) models have similar longitudinal locations (difference <100 km), implying the longitudinal uncertainty of mapping to be small. The latitudinal uncertainty can be inferred by referring to the open-closed field line boundary as estimated using the 150 m/s spectral width boundary [e.g., *Baker et al.*, 1995, 1997; *Chisham and Freeman*, 2003]. And T89 has given the smallest latitudinal uncertainty for the studied events. We surveyed years 2014-2016 during the months when the satellite apogee was on the dayside, and present three events in the paper.

The ionospheric signature of reconnection jets includes fast anti-sunward flows moving across the open-closed field line boundary. We obtain the flow velocity vectors by merging line-of-sight (LOS) measurements at the radar common FOVs [*Ruohoniemi and Baker*, 1998], and these merged vectors reflect the true ionospheric convection velocity. However, the radar common FOVs are hundreds of km wide only, which can be too small to cover the full azimuthal extent of the reconnection-related flows (which are up to thousands of km wide). We therefore also reconstruct the velocity field using the Spherical Elementary Current Systems (SECS) method [*Amm et al.*, 2010]. Similar to the works by *Ruohoniemi et al.* [1989] and *Bristow et al.* [2016], the SECS method reconstructs a divergence-free flow pattern using all LOS velocity data. We refer to these velocities as SECS velocities. The accuracy of SECS velocities can be validated by comparing to the LOS measurements and the merged vectors. SECS velocities work best in regions with dense echo coverage and those around sparse echoes are not reliable and thus are excluded from our analysis.

The third way of obtaining a velocity field is Spherical Harmonic Fit (SHF). This method uses the LOS measurements and a statistical convection model to fit the distribution of electrostatic potential, which is expressed as a sum of spherical harmonic functions [*Ruohoniemi and Baker*, 1998]. The statistical model employed here is *Cousins and Shepherd* [2010]. While this method may suppress small or meso-scale velocity details, such as, sharp flow gradients or flow vortices, we compare SHF velocities with the LOS measurements and merged vectors to determine how well the SHF velocities depict the velocity details.

As seen in our observations presented below, the longitudinal profile of the fast anti-sunward ionospheric flows has a near bell shaped curve. We measure the extent based on full width at half maximum (FWHM) of the profile at 1° poleward of the open-closed field line boundary. The choice of FWHM is analogous to *Shay et al.* [2003], where the reconnection extent is measured as regions of electron speed above half of the peak electron flow speed during reconnection. The choice is also supported by magnetopause observations, where we find that ionospheric flows with a speed above half of the peak flow speed map to jets consistent with Walen relation, while those with a speed below map to jets much slower than the Walen relation (Section 3.1). However, it should be noted that the magnitude of the widths is always dependent on the threshold used, and that half maximum is very likely not the only sensible threshold. Using FWHM excludes ionospheric flows with a speed below half of the peak flow speed. Those flows, if related to reconnection, associate with comparatively slow generation of open magnetic flux and low contribution to geomagnetic activity.

Among the three presented events, the time separations of magnetopause crossings by two satellites are 1, 2, and 30 min. While the time separation for the third case is somewhat long, we distinguish the spatial and temporal effects using the radar data. Although the three events occurred under similar IMF Bz conditions, the reconnection-related flows in the ionosphere had an azimuthal extent varying from a few hundred km (Sections 3.1-3.2) to more than a thousand km wide (Section 3.3). This corresponds to reconnection of a few to >10 Re wide indicating that both spatially patchy (a few Re) and spatially continuous and extended reconnection (>10 Re) are possible forms of active reconnection at the magnetopause. Interestingly, the extended reconnection was found to arise from a spatially localized patch that spreads azimuthally. Potential effects of IMF Bx and By on the reconnection extent are discussed in Section 4.

Note that reconnection can happen over various spatial and temporal scales and our space-ground approach can resolve reconnection that are larger than 0.5 Re and persist longer than a few minutes. This is limited by the radar spatial and temporal resolution, and the magnetosphere-ionosphere coupling time which is usually 1-2 min [e.g. *Carlson et al.*, 2004]. This constraint is not expected to impair the result because reconnection above this scale has been found to occur commonly in statistics (see the Introduction section for spatial and *Lockwood and Wild* [1993], *Kuo et al.* [1995], *Fasel* [1995], and *McWilliams et al.* [1999] for temporal characteristics).

## 3. Observations

3.1. Spatially patchy reconnection active at one satellite only

3.1.1 In-situ satellite measurements

On February 2, 2013, THA and THE made simultaneous measurements of the dayside magnetopause with a 1.9 Re separation in the Y direction around 21:25 UT. The IMF condition is displayed in Figure 1a and the IMF was directed southward. The satellite location in the GSM coordinates is displayed in Figure 1b, and the measurements are presented in Figure 2. The magnetic field and the ion velocity components are displayed in the LMN boundary normal coordinate system, where *L* is along the outflow direction, *M* is along the X-line, and *N* is the current sheet normal. The coordinate system is obtained from the minimum variance analysis of the magnetic field at each magnetopause crossing [*Sonnerup and Cahill*, 1967]. Figures 2g-p show that both satellites passed from the magnetosheath into the magnetosphere, as seen as the sharp changes in the magnetic field, the ion spectra, and the density (shaded in pink).

As THE crossed the magnetopause boundary layer (2122:57-2123:48 UT), it detected a rapid, northward-directed plasma jet within the region where the magnetic field rotated (Figures 2g and 2j). The magnitude of this jet relative to the sheath background flow reached 262 km/s at its peak, which was 72% of the predicted speed of a reconnection jet by the Walen relation (366 km/s, not shown). The angle between the observed and predicted jets was 39°. THE also detected kinetic signatures of reconnection. The ion distributions in Figure 2k showed a distorted D-shaped distribution similar to the finding of by *Broll et al.* [2018]. The distortion is due to particles traveling in the field-aligned direction from the reconnection site to higher magnetic field region, and *Broll et al.* [2018] estimated the traveling distance to be a few Re for the observed level of distortion.

THA crossed the magnetopause one to two minutes later than THD (2124:48-2125:13 UT).

While it still identified a plasma jet at the magnetopause (Figures 2l and 2o), the jet speed was significantly smaller than what was predicted for a reconnection jet (80 km/s versus 380 km/s in the *L* direction). The observed jet was directed 71° away from the prediction. The ion distributions deviated from clear D-shaped distributions (Figure 2p). This suggests that the reconnection jet at THE likely did not extend to THA.

### 3.1.2 Ground radar measurements

The velocity field of the dayside cusp ionosphere during the satellite measurements is shown in Figures 2a-c. Figure 2a shows the radar LOS measurements at 21:25 UT, as denoted by the color tiles, and the merged vectors, as denoted by the arrows. The colors of the arrows indicate the merged velocity magnitudes, and the colors of the tiles indicate the LOS speeds that direct anti-sunward (those project to the sunward direction appear as black). Fast (red) and anti-sunward flows are the feature of our interest. One such of this flow can be identified in the pre-noon sector, which had a speed of ~800 m/s and was directed poleward and westward. As the merged vector arrows indicate, the velocity vectors have a major component close to the INV beam directions and thus the INV LOS velocities reflect the flow distribution. The flow crossed the open-closed field line boundary, which was located at 78° MLAT based on the spectral width (Figure 2d and S1). This flow thus meets the criteria of being an ionospheric signature of magnetopause reconnection jets. Another channel of fast flow was present in the post-noon sector. This post-noon flow was directed more azimuthally and was increasingly separated from the pre-noon flow as it moved away from the noon (see the region of slow velocities at >79° MLAT around noon). The difference in flow trajectories implies that these flows were driven by different magnetic tension forces. They also evolved differently over time as seen in Figure 2e which is discussed below. The flows thus likely originated from two reconnection regions that were associated with different magnetic field topologies and different temporal variabilities. Since the satellites were located in the pre-noon sector we focus on the pre-noon flow below.

The flow had a limited azimuthal extent. The extent is determined at half of the maximum flow speed, which was ~400 m/s. Figure 2f discussed below shows a more quantitative estimate of the extent. In Figure 2a, we mark the eastern and western boundaries with the dashed magenta lines, across which the LOS velocities dropped from red to blue/green colors.

Figure 2b shows the SECS velocities, denoted by the arrows. The SECS velocities reasonably reproduced the spatial structure of the flows seen in Figure 2a. The flow boundaries were marked by the dashed magenta lines, across which the flow speed dropped from red to blue.

The velocity field reconstructed using the SHF velocities is shown in Figure 2c (obtained through the Radar Software Toolkit (http://superdarn.thayer.dartmouth.edu/software.html)). This is an expanded view of the global convection maps in Figure S2 focusing on the dayside cusp. Comparing Figures 2c and S2 reveals that the employed radars listed in Section 2 have contributed to the majority of the backscatters on the dayside. This is because this event (same for the following two events) occurred under non-storm time, where the open-closed field line was confined within the FOVs of the radars used. During storm time the boundary expands to lower latitude where backscatter from a wider network of radars may be available. The SHF velocities also captured the occurrence of two flows in the pre- and post-noon sectors, respectively, although the orientation of the flows were slightly different from Figure 2a or 2b. The difference is likely due to the contribution from the statistical potential distribution under the southward IMF. The flow western and eastern boundaries were again marked by the dashed magenta lines.

Figure 2d shows spectral width measurements. Large spectral widths can be produced by soft

(~100 eV) electron precipitation [*Ponomarenko et al.*, 2007], and evidence has shown that the longitudinal extent of large spectral widths correlates with the extent of PMAFs [*Moen et al.*, 2000] and of poleward flows across the open-closed field line boundary [*Pinnock and Rodger*, 2001]. Large spectral widths thus have the potential to reveal the reconnection extent. For the specific event under examination, the region of large spectral widths, appearing as red color, spanned from 10.5 to 14.5 h MLT if we count the sporadic scatters in the post-noon sector. This does not contradict the flow width identified above because the wide width reflects the summed width of the pre- and post-noon flows. In fact a more careful examination shows that there might exist two dark red regions (circled in red, the red dashed line is due to the discontinuous backscatters outside the INV FOV) embedded within the ~200-m/s spectral widths. These two regions had slightly higher spectral widths than the surrounding (by ~20-50 m/s) and possibly corresponded to the two flows.

Figures 2a-c all observed a channel of fast anti-sunward flow in the pre-noon sector of the high latitude ionosphere, and the flow had a limited azimuthal extent. If the flow corresponded to a magnetopause reconnection jet, the reconnection jet is expected to span over a limited local time range. This is consistent with the THEMIS satellite observation in Section 3.1.1, where THE at Y = -2.9 Re detected a clear reconnection jet, while THA at Y = -4.8 Re did not. In fact, if we project the satellite location to the ionosphere through field line tracing under the T89 model, THE was positioned at the flow longitude, while THA was to the west of the flow embedded in weak convection (Figure 2a).

While this paper primarily focuses on the spatial extent of reconnection, the temporal evolution can be obtained from the time series plot in Figure 2e. Figure 2e presents the northward component of the SECS velocity along 79° MLAT (just 1° poleward of the open-closed field line boundary) as functions of magnetic local time (MLT) and time. Here we only show the northward component of the SECS velocity as this component represents reconnecting flows across an azimuthally-aligned open-closed field line boundary. Similar to the snapshots, the flow of our interest appears as a region of red color. The time and the location where THA and THE crossed the magnetopause are marked by the crosses. The pre-noon flow emerged from a weak background from 2122 UT and persisted for ~>30 min, while the post-noon flow only lasted for ~10 min. Minutes following the onset the pre-noon flow spread in width, where the western boundary of the red color moved from 10.7 to 10.5 h MLT, and the eastern boundary moved to 11.2 to 11.5 h MLT. After 2134 UT the spreading ceased and the entire flow moved westward (the western boundary moved beyond the FOV). Hence the reconnection-related ionospheric flow, once formed, has spread in width and displaced westward. The spreading behavior is similar to events studied by Zou et al. [2018], and is interpreted to relate to spreading of the reconnection extent seen in simulation studies (see introduction). The spreading has also been noticed in the other two events (see Section 3.3), indicating that this could be a common development feature of the reconnection-related flows.

A consequence of the flow temporal evolution is that THA, which was previously outside the reconnection-related flow, became immersed in the flow from 2130 UT, while THE, which was previously inside the flow, was left outside from 2142 UT (Figure 2e). This implies that at the magnetopause the reconnection has spread azimuthally sweeping across THA, and has slid in the –y direction away from THE. This is in perfect agreement with satellite measurements shown in Figures 2q-z. Figures 2q-z presents subsequent magnetopause crossings made by THA and THE following the crossings in Figures 2g-p. THA detected an Alfvenic reconnection jet and a clear D-shape ion distribution, and THE detected a jet much slower than the Alfvenic speed and an ion distribution without a clear D-shape. This corroborates the connection between the in-situ reconnection jet with the fast anti-sunward ionospheric flow, and reveals the dynamic evolution of reconnection in the local time direction. On the other hand, this also sheds light on the nature of the slow convection outside the fast flow, which corresponds to sub-Alfvenic jets at the magnetopause.

We quantitatively determine the flow extent in Figure 2f. Figure 2f shows the profile of the northward component of the SECS velocity at 2129 UT as a function of the distance from magnetic noon. The 2129 UT is the time when the flow extent has slowed down from spreading and stabilized. The profile should theoretically be taken just poleward of the open-closed field line boundary. In practice we smooth the velocity in latitude with a 1° window and take measurements 1° poleward of the open-closed field line boundary. The profile has a near bell shaped curve, and the FWHM was 200 km at an altitude of 250 km. Also shown is the INV LOS velocity profile, which is obtained in a similar manner as the SECS one. The LOS velocity profile also gives a narrow FWHM, which was 280 km.

While it is commonly assumed that the extent of reconnection jets reflects the extent of reconnection, we test the assumption by calculating the distribution of reconnection electric field in Figure 3. Reconnection electric field can be estimated by measuring the flow across the open-closed field line boundary in the reference frame of the boundary [*Pinnock et al.*, 2003; *Freeman et al.*, 2007; *Chisham et al.*, 2008], and we follow this procedure to derive the its distribution across local time. A close-up presentation of the open-closed field line boundary is shown in Figures 3a-c around the space-ground conjunction time and longitude. The open-closed field line boundary, drawn as the dashed black line, is identified following *Chisham and Freeman* [2003, 2004] and *Chisham et al.* [2004b, 2005a, 2005b, 2005c]. The boundary was almost along a constant magnetic latitude. The motion of the boundary is obtained by inspecting the time series of the spectral width measurements along each radar beam and examples are given for INV beams 4, 7, and 10 in Figures 3d-f. Subtracting the speed of the boundary from that of the flow (in the rest frame) across the boundary gives the flow speed in the reference frame of the boundary. Assuming that the flow is $E \times B$ drift, electric field can be derived and this is the ionosphere-mapped reconnection electric field. The flow speed across the boundary is taken from the 1°-averaged speed at the boundary latitude (similar to *Chisham et al.* [2008]). Note that a precise determination of the boundary motion could be subject to radar spatial and temporal resolution and the error can be as large as 300 m/s or 15 mV/m.

As shown in Figure 3g, the profile of the reconnection electric field had a peak in the azimuthal direction with a limited FWHM, and the FWHM is essentially the same as the flow width just poleward of the boundary (difference being less than the radar spatial resolution) This establishes the relation between our measure of the reconnection jet extent and the extent of reconnection of high reconnection rates. Regions of high reconnection rates are localized, although those of low reconnection rates (>0 mV/m) can extend over a much broader region. For example, the western boundary of non-zero reconnection rates was located just at the edge of INV FOV (considering the 15 mV/m uncertainty), and the eastern edge extended beyond INV FOV, likely into where the post-noon flow was originated from. A lower estimate of the extent of non-zero reconnection rates is therefore ~4 h MLT. It is likely that there were two components of reconnection at different scales: broad and low-rate background reconnection, and embedded high-rate reconnection.

To infer the reconnection extent at the magnetopause, we project the flow extent based on the SECS in the ionosphere to the equatorial plane. The result suggests that the reconnection local time extent was ~2 Re.

### 3.2. Spatially patchy reconnection active at both satellites

#### 3.2.1. In-situ satellite measurements

On April 19, 2015, under a southward IMF (Figure 4a), THA and THE crossed the magnetopause nearly simultaneously (<2 min lag) with a 0.5 Re separation in Y (Figure 4b). They passed from the magnetosheath into the magnetosphere. Both satellites observed jets in the $V_L$ component at the magnetopause (Figures 5g-p). The jet at THA at ~1828:05 UT had a speed of 84% of and an angle within ~15° from the Walen prediction. The jet at THE at ~1826:25 UT had a speed of 95% of and an angle of ~29° from the Walen prediction. The ion distributions at THA and THE exhibit clear D-shaped distributions. Reconnection thus occurred at both local times.

#### Section 3.2.2. Ground radar measurements

During the satellite measurements, the radars observed a channel of fast anti-sunward flow around magnetic noon (Figures 5a-c). The flow crossed the open-closed field line boundary at 77° MLAT, and qualifies for an ionospheric signature of magnetopause reconnection jets. The flow direction was nearly parallel to the RKN radar beams, and therefore the RKN LOS measurements in Figure 5a approximated to the 2-d flow speed. The flow eastern boundary can be identified as where the velocity dropped from red/orange to blue (dashed magenta line). Determining the flow western boundary requires more measurements of the background convection velocity, which is beyond the RKN FOV. But we infer that the western boundary did not extend more than 1.5 h westward beyond the RKN FOV because the PGR and INV echoes there showed weakly poleward and equatorward LOS speeds around the open-closed field line boundary. The CLY radar data further indicated that the anti-sunward flow had started to rotate westward immediately beyond the RKN FOV. This is because the CLY LOS velocities measured between the RKN and INV radar FOVs were larger for more east-west oriented beams (appearing as yellow color) than for more north-south oriented beams (green color). The rotation likely corresponds to the vortex at the flow western boundary as sketched in *Oksavik et al.* [2004].

The more precise location of the western boundary can be retrieved from the SECS velocities in Figure 5b and the SHF velocities in Figure 5c. The SECS velocities present a flow channel very similar to that in Figure 5a, while the flow channel in the SHF velocities was more azimuthally-aligned than in Figures 5a-b. It can be seen that across the flow western boundary the flow direction reversed. The equatorward-directed flows are interpreted as the return flow of the poleward flows, as sketched in *Southwood* [1987] and *Oksavik et al.* [2004].

The determined flow extent agrees with the extent of the cusp in Figure 5d. The high spectral widths associated with the cusp were located at the western half of the RKN FOV. They extended westward beyond the RKN FOV into CLY far range gates, where they dropped from red to green color. This is consistent with the inferred location and extent of the anti-sunward fast flow.

The flow of our interest just emerged from a weak background at the time when the THEMIS satellites crossed the magnetopause (Figure 5e). This implies that the related reconnection just activated at the studied local time. The flow spread azimuthally until 1833 UT when it stabilized. We quantify the stabilized flow extent and the reconnection electric field extent (Figure 5f) in a similar way as Figure 2f and Figure 3g. The FWHM of the flow is determined to be 432 and 336 km based on the SECS and RKN LOS data respectively. While the reconnection electric field had data gaps due to the limited coverage and backscatter availability at near range gate, it implies a western boundary of FWHM consistent with the flow slightly poleward of it. This is also the western boundary of non-zero reconnection rates considering the 15-mV/m uncertainty. The eastern boundary extended beyond RKN FOV. The FWHM of the SECS flow profile corresponds to ~4 Re in the equatorial plane.

The fact that the fast anti-sunward flow had a limited azimuthal extent around magnetic noon implies that the corresponding magnetopause reconnection should span over a limited local time range around the noon. This is consistent with the THEMIS satellite observation in Section 3.2.1, where reconnection was active at Y = 0.7 (THA) and 0.2 Re (THE). Projecting THA and THE locations to the ionosphere reveals that both satellite footprints were located within the flow longitudes. Therefore the reconnection at the two satellites was part of the same reconnection around the subsolar point of the magnetopause. (The THE footprint was equatorward of THA because the X location of THE was closer to the Earth than THA. The magnetopause was expanding and it swept across THE and then THA.) The reconnection further extended azimuthally beyond the two satellite locations, reaching a full length of ~4 Re.

### 3.3. Spatially continuous and extended reconnection active at both satellites

#### 3.3.1. In-situ satellite measurements

On Apr 29, 2015, under a prolonged and steady southward IMF (Figure 6a), THA and THE crossed the magnetopause successively with a time separation of ~30 min. The locations of the crossings were separated by 0.1-0.2 Re in the Y direction (Figure 6b). The satellites passed from the magnetosphere into the magnetosheath, and the magnetic field data suggest that the satellites crossed the current layer multiple times before completely entering the magnetosheath (Figures 6i-r). We therefore only display the magnetic field and the plasma velocity in the GSM coordinates. Both satellites detected multiple flow jets, all agreeing with the Walen prediction with $\Delta V^* > 0.5$. For example, the jet at 1849-1850 UT measured by THA had a speed with 80% of and angle with 9° from the Walen prediction, and the jet at 1920-1922 UT by THE had a speed with 83% of and an angle with 1° from the Walen prediction. The ion distributions at THA and THE exhibit clear D-shaped distributions.

### 3.3.2. Ground radar measurements

In the ionosphere, the radars detected a fast anti-sunward flow as an ionospheric signature of the magnetopause reconnection jet (Figures 7a-c). The flow had a broad azimuthal extent, as delineated by the dashed magenta lines (Figure 7a). A similar flow distribution is found in the SECS velocities (Figure 7b), and the SHF velocities (Figure 7c). The flow propagated into the polar cap as one undivided channel (as opposed to Section 3.1.2), implying that it was one flow structure at least to the resolution the radars can resolve. Corresponding to the broad extent of the flow, the cusp had a broad extent (Figure 7d). The cusp continuously spanned across the INV and RKN FOVs and its western and eastern edges coincided with the western and eastern boundaries of the flow, supporting our delineation of the flow extent.

The wide flow channel in the ionosphere implies that the corresponding magnetopause reconnection jet should be wide in local time. Based on the flow distribution, we infer that much of the reconnection should be located on the pre-noon sector, except that the eastern edge can extend across the magnetic noon meridian to the early post-noon sector. This inference is again consistent with the inference from the THA and THE measurements that the reconnection extended at least over the satellite separation (Y = -0.2 (THA) and 0 Re (THE)). Note, however, that the distance between THA and THE only covered <2% of the reconnection extent determined from the ionosphere flow. While the satellite configuration and measurements here were similar to those in Section 3.2, the extent of reconnection was fundamentally different. This suggests that it is difficult to obtain a reliable estimate of the reconnection extent without the support of 2-d measurements and that satellites alone also cannot differentiate spatially extended reconnection from spatially patchy reconnection.

The flow temporal evolution is shown in Figures 7e, where the velocities are the northward component of the SECS data. An overall wide flow channel is seen during the time interval of our interest with the eastern and western boundaries located at ~12.0-12.5 and ~8.0-8.7 h MLT, respectively. But between the two satellite observations, the flow experienced an interesting variation. The velocity at 9.3-12.0 h MLT dropped by 100-200 m/s during 1902-1912 UT (red color turned orange, yellow, and then green), while the velocity at 8.6-9.3 h MLT did not change substantially. The velocity enhanced again from 1912 UT. The enhancement centered at 10.7 h MLT and spread azimuthally towards east and west. The enhancement spread by 0.7 h MLT over 14 min at its eastern end (marked by the dashed black line), suggesting a spreading speed of 275 m/s. The enhancement spread by 1.2 h MLT at its western end, suggesting a spreading speed of 471 m/s. It should be noted that the all three components of the IMF stayed steady for an extended time (Figure 8, discussed below in Section 4), and thus the evolution of the flow/reconnection was unlikely to be externally driven.

This sequence of changes gives an important implication that the spatially extended reconnection was a result of spreading of an initially patchy reconnection. If we map the spreading in the ionosphere to the magnetopause, the spreading occurred bi-directionally and at a speed of 15 and 26 km/s in the east and west directions based on field-line mapping under the T89 model (the mapping factor was 55). Such an observation is similar to what has recently been reported by *Zou et al.* [2018], where the reconnection also spreads bi-directionally at a speed of a few tens of km/s. However, the spreading in *Zou et al.* [2018] occurs following a southward turning of the IMF, while the spreading here occurred without IMF variations. The mechanism of spreading is explained either as motion of the current carriers of the reconnecting current sheet or as propagation of the Alfven waves along the guide field [*Huba and Rudakov*, 2002; *Shay et al.* 2003; *Lapenta et al.*, 2006; *Nakamura et al.*, 2012; *Jain et al.*, 2013].

It should be noted that reconnection spreading can be a common process of reconnection that is not limited to extended reconnection. It also occurs for patchy reconnection as seen in Sections 3.1 and 3.2. The spreading speeds were similar across the three events but the duration of the spreading process was two to three times longer in the spatially extended than the spatially patchy reconnection events. For the extended reconnection, the spreading process persisted for 14 min expanding the extent by 5-6 Re.

Figure 7f quantifies the extent of the flow and reconnection electric field. The FWHM extent was 1320 km based on the SECS data. Despite the presence of the data gaps, the LOS measurements suggest a western and eastern boundary consistent with the SECS data. The reconnection electric field had a similar FWHM to the flow although regions of non-zero reconnection rates again extended beyond the available coverage indicating an overall extent >4 h MLT. The extent corresponds to a reconnection extent of ~11 Re.

## 4. Discussion

The above events definitely show that the local time extent of magnetopause reconnection can vary from a few to >10 Re. Here we investigate whether and how the extent may depend on the upstream driving conditions. Figure 8 presents the IMF, the solar wind velocity, and the solar wind pressure taken from the OMNI data for the three events. The red vertical lines mark the times when the reconnection was measured. The three events occurred under similar IMF field strengths (5-6 nT), similar IMF Bz components (-2-3 nT), and similar dynamic pressures (1-2 nPa), implying that the different reconnection extents were unlikely due to these parameters. The solar wind speeds had a slight decreasing trend as the reconnection extent increased. This is different from *Milan et al.* [2016], who identified a large solar wind speed as a cause of a large reconnection extent. However, *Milan et al.* [2016] studied reconnection under very strong IMF driving conditions when |B| ~15 nT, while our events occurred under a more typical moderate driving (|B| ~5-6 nT).

The spatially patchy reconnection events had an IMF Bx of a larger magnitude than the extended reconnection event did (4 vs. 0 nT). The spatially patchy reconnection events also had an IMF By component of a smaller magnitude (2 vs. 5 nT, and therefore a clock angle closer to 180°), and with more variability on time scales of tens of minutes, than the extended reconnection event. The IMF Bx and By components are known to modify the magnetic shear across the magnetopause and to affect the occurrence location of reconnection. Studies have found that at dayside low latitude magnetopause small $\left|B_y|/|B_z\right|$ relates to anti-parallel and large $\left|B_y|/|B_z\right|$ to component reconnection [*Coleman et al.*, 2001; *Chisham et al.*, 2002; *Trattner et al.*, 2007]. Large $|B_x|/|B|$, i.e. cone angle, also favors formation of high-speed magnetosheath jets [*Archer and Horbury*, 2013; *Plaschke et al.*, 2013] of a few Re in scale size, resulting in a turbulent magnetosheath environment for reconnection to occur [*Coleman, and Freeman*, 2005]. The steady IMF condition may allow reconnection to spread across local times unperturbedly, eventually reaching a wide extent. Thus our preliminary analysis suggests that the reconnection extent may depend on the IMF orientation and steadiness, although whether and how they influence the extent needs to be further explored.

## 5. Summary

We carefully investigate the local time extent of magnetopause reconnection by comparing the measurements of reconnection jets by two THEMIS satellites and three ground radars. When reconnection jets are only observed at one of the two satellite locations, only the ionosphere conjugate to this spacecraft shows a channel of fast anti-sunward flow. When reconnection jets are observed at both spacecraft and the spacecraft are separated by <1 Re, the ionosphere conjugate to both spacecraft shows a channel of fast anti-sunward flow. The fact that the satellite locations are mapped to the same flow channel suggests that the reconnection is continuous between the two satellites, and that it is appropriate to take the satellite separation as a lower limit estimate of the reconnection extent. Whether reconnection can still be regarded as continuous when the satellites are separated by a few or > 10 Re is questionable, and needs to be examined using conjunctions with a larger satellite separation than what have been presented here.

The reconnection extent is measured as the FWHM of the ionospheric flow. In the three conjunction events, the flows have FWHM of 200, 432, and 1320 km in the ionosphere, which corresponds to ~2, 4, and 11 Re at the magnetopause (under the T89 model) in the local time direction. The flow extent is confirmed to be related to reconnection of high reconnection electric field. The result provides strong observational evidence that magnetopause reconnection can occur over a wide range of extents, from spatially patchy (a few Re) to spatially continuous and extended (>10 Re). Interestingly, the extended reconnection is seen to initiate from a patchy reconnection, where the reconnection grows by spreading across local time. The speed of spreading is 41 km/s summing the westward and eastward spreading motion, and the spreading process persists for 14 min broadening the extent by 5-6 Re.

Based on the three events studied in this paper, the reconnection extent may be affected by the IMF orientation and steadiness, although the mechanism is not clearly known. For the observed modest solar wind driving conditions, the spatially extended reconnection is suggested to occur under a smaller IMF Bx component, and a larger and steadier IMF By component than the spatially patchy reconnection. The IMF strength, the Bz component, and the solar wind velocity and pressure are about the same for the extended and the patchy reconnection. This finding, however, could be limited by the number of events under analysis, and further study is needed to achieve an understanding of how solar wind controls reconnection extent. Reconnection can vary with time, even under steady IMF driving conditions.

**Acknowledgments.** This research was supported by the NASA Living With a Star Jack Eddy Postdoctoral Fellowship Program, administered by UCAR's Cooperative Programs for the Advancement of Earth System Science (CPAESS), NASA grant NNX15AI62G, NSF grants PLR-1341359 and AGS-1451911, and AFOSR FA9550-15-1-0179 and FA9559-16-1-0364. The THEMIS mission is supported by NASA contract NAS5-02099. SuperDARN is a collection of radars funded by national scientific funding agencies. SuperDARN Canada is supported by the Canada Foundation for Innovation, the Canadian Space Agency, and the Province of Saskatchewan. We thank Tomoaki Hori for useful discussion on the SECS technique. Data products of the SuperDARN, THEMIS, and OMNI are available at http://vt.superdarn.org/, http://themis.ssl.berkeley.edu/index.shtml, and GSFC/SPDF OMNIWeb website.

Reference

Amm, O., Grocott, A., Lester, M. and Yeoman, T. K.: Local determination of ionospheric plasma convection from coherent scatter radar data using the SECS technique, J. Geophys. Res., 115, A03304, doi:10.1029/2009JA014832, 2010.

Angelopoulos, V.: The THEMIS mission, Space Sci. Rev., 141, 5–34, doi:10.1007/s11214-008-

9336-1, 2008.

Archer, M. O. and Horbury, T. S.: Magnetosheath dynamic pressure enhancements: occurrence and typical properties, Ann. Geophys., 31, 319-331, https://doi.org/10.5194/angeo-31-319-2013, 2013.

Auster, H. U., et al.: The THEMIS fluxgate magnetometer, *Space Sci. Rev.*, **141**, 235–264, 2008.

Baker, K. B., Dudeney, J. R., Greenwald, R. A., Pinnock, M., Newell, P. T., Rodger, A. S., Mattin, N. , and Meng, C.-I.: HF radar signatures of the cusp and low-latitude boundary layer, J. Geophys. Res., 100(A5), 7671–7695, doi:10.1029/94JA01481, 1995.

Baker, K. B., Rodger, A. S., and Lu, G.: HF-radar observations of the dayside magnetic merging rate: A Geospace Environment Modeling boundary layer campaign study, J. Geophys. Res., 102(A5), 9603–9617, doi:10.1029/97JA00288, 1997.

Bobra, M. G., Petrinec, S. M., Fuselier, S. A., Claflin, E. S., and Spence, H. E.: On the solar wind control of cusp aurora during northward IMF, Geophys. Res. Lett., 31, L04805, doi:10.1029/2003GL018417, 2004.

Bristow, W. A., Hampton, D. L., and Otto, A.: High-spatial-resolution velocity measurements derived using Local Divergence-Free Fitting of SuperDARN observations, J. Geophys. Res. Space Physics, 121, 1349–1361, doi:10.1002/2015JA021862, 2016.

Chisham, G., Coleman, I. J., Freeman, M. P., Pinnock, M., and Lester, M.: Ionospheric signatures of split reconnection X-lines during conditions of IMF Bz < 0 and |By|/|Bz|: Evidence for the antiparallel merging hypothesis, J. Geophys. Res., 107(A10), 1323, doi:10.1029/2001JA009124, 2002.

Chisham, G., and Freeman, M. P.: A technique for accurately determining the cusp-region polar cap boundary using SuperDARN HF radar measurements, Ann. Geophys., 21, 983–996, 2003.

Chisham, G., Freeman, M. P., Coleman, I. J., Pinnock, M., Hairston, M. R., Lester, M., and Sofko, G.: Measuring the dayside reconnection rate during an interval of due northward interplanetary magnetic field, Ann. Geophys., 22, 4243–4258, 2004.

Chisham, G., and M. P. Freeman: An investigation of latitudinal transitions in the SuperDARN Doppler spectral width parameter at different magnetic local times, Ann. Geophys., 22, 1187–1202, 2004.

Chisham, G., Freeman, M. P., and Sotirelis, T.: A statistical comparison of SuperDARN spectral width boundaries and DMSP particle precipitation boundaries in the nightside ionosphere, Geophys. Res. Lett., 31, L02804, doi:10.1029/2003GL019074, 2004b.

Chisham, G., Freeman, M. P., Sotirelis, T., Greenwald, R. A., Lester, M., and Villain J.-P.: A statistical comparison of SuperDARN spectral width boundaries and DMSP particle precipitation boundaries in the morning sector ionosphere, Ann. Geophys., 23,733–743, 2005a.

Chisham, G., Freeman, M. P., Sotirelis, T., and Greenwald, R. A.: The accuracy of using the spectral width boundary measured in off-meridional SuperDARN HF radar beams as a proxy for the open-closed field line boundary, Ann. Geophys., 23, 2599–2604, 2005b.

Chisham, G., Freeman, M. P., Lam, M. M., Abel, G. A., Sotirelis, T., Greenwald, R. A., and Lester, M.: A statistical comparison of SuperDARN spectral width boundaries and DMSP particle precipitation boundaries in the afternoon sector ionosphere, Ann. Geophys., 23, 3645–3654, 2005c.

Chisham, G., et al.: Remote sensing of the spatial and temporal structure of magnetopause and magnetotail reconnection from the ionosphere, Rev. Geophys., 46, RG1004, doi:10.1029/2007RG000223, 2008.

Coleman, I. J., Chisham, G., Pinnock, M., and Freeman, M. P., An ionospheric convection signature of antiparallel reconnection, J. Geophys. Res., 106, 28,995–29,007, 2001.

Coleman, I. J., and Freeman, M. P.: Fractal reconnection structures on the magnetopause, Geophys. Res. Lett., 32, L03115, doi:10.1029/2004GL021779, 2005.

Cousins, E. D. P., and Shepherd, S. G.: A dynamical model of high‐latitude convection derived from SuperDARN plasma drift measurements, *J. Geophys. Res.*, 115, A12329, doi:10.1029/2010JA016017, 2010.

Crooker, N. U., Dayside merging and cusp geometry, J. Geophys. Res., 84(A3), 951–959, doi:10.1029/JA084iA03p00951, 1979.

Crooker, N. U., F. R. Toffoletto, and M. S. Gussenhoven, Opening the cusp, J. Geophys. Res., 96(A3), 3497–3503, doi: 10.1029/90JA02099, 1991.

Denig, W. F., Burke, W. J., Maynard, N. C., Rich, F. J., Jacobsen, B., Sandholt, P. E., Egeland, S., Leontjev, A., and Vorobjev, V. G.: Ionospheric signatures of dayside magnetopause transients: A case study using satellite and ground measurements, *J. Geophys. Res.*, **98**(A4), 5969–5980, doi:10.1029/92JA01541, 1993.

Dorelli, J. C., Bhattacharjee, A., and Raeder, J.: Separator reconnection at Earth's dayside magnetopause under generic northward interplanetary magnetic field conditions, J. Geophys. Res., 112, A02202, doi:10.1029/2006JA011877, 2007.

Dunlop, M. W., et al.: Magnetopause reconnection across wide local time, *Ann. Geophys.*, **29**, 1683–1697, doi:10.5194/angeo-29-1683-2011, 2011.

Elphic, R. C., Lockwood, M., Cowley, S. W. H., and Sandholt, P. E.: Flux transfer events at the magnetopause and in the ionosphere, Geophys. Res. Lett., 17, 2241, 1990.

Fasel, G. J. (1995), Dayside poleward moving auroral forms: A statistical study, *J. Geophys. Res.*, 100(A7), 11891–11905, doi: 10.1029/95JA00854.

Fear, R. C., Milan, S. E., Fazakerley, A. N., Lucek, E. A., Cowley, S. W. H., and Dandouras, I.: The azimuthal extent of three flux transfer events, Ann. Geophys., 26, 2353-2369, https://doi.org/10.5194/angeo-26-2353-2008, 2008.

Fear, R. C., Milan, S. E., Lucek, E. A., Cowley, S. W. H., and Fazakerley, A. N.: Mixed azimuthal scales of flux transfer events, in *The Cluster Active Archive – Studying the Earth's Space Plasma Environment*, Astrophys. Space Sci. Proc., edited by H. Laakso, M. Taylor, and C. P. Escoubet, pp. 389–398, Springer, Dordrecht, Netherlands, doi:10.1007/978-90-481-3499-1_27, 2010.

Freeman, M. P., G. Chisham, and I. J. Coleman (2007), Remote sensing of reconnection, in Reconnection of Magnetic Fields, edited by J. Birn and E. Priest, chap. 4.6, pp. 217–228, Cambridge Univ. Press, New York.

Fuselier, S. A., Frey, H. U., Trattner, K. J., Mende, S. B., and Burch, J. L.: Cusp aurora dependence on interplanetary magnetic field Bz, J. Geophys. Res., 107(A7), 1111, doi:10.1029/2001JA900165, 2002.

Fuselier, S. A., Mende, S. B., Moore, T. E., Frey, H. U., Petrinec, S. M., Claflin, E. S., and Collier, M. R.: Cusp dynamics and ionospheric outflow, in Magnetospheric Imaging—The Image Mission, edited by J. L. Burch, Space Sci. Rev., 109, 285, doi:10.1023/B:SPAC.0000007522.71147.b3, 2003.

Fuselier, S. A., Trattner, K. J., Petrinec, S. M., Owen, C. J., and Rème, H., Computing the reconnection rate at the Earth's magnetopause using two spacecraft observations, J. Geophys. Res., 110, A06212, doi:10.1029/2004JA010805, 2005.

Fuselier, S. A., Petrinec, S. M., and Trattner, K. J.: Antiparallel magnetic reconnection rates at the Earth's magnetopause, J. Geophys. Res., 115, A10207, doi:10.1029/2010JA015302, 2010.

Glocer, A., Dorelli, J., Toth, G., Komar, C. M., and Cassak, P. A.: Separator reconnection at the magnetopause for predominantly northward and southward IMF: Techniques and results, J. Geophys. Res. Space Physics, 121, 140–156, doi:10.1002/2015JA021417, 2016.

Goertz, C. K., Nielsen, E., Korth, A., Glassmeier, K. H., Haldoupis, C., Hoeg, P., and Hayward, D.: Observations of a possible ground signature of flux transfer events, J. Geophys. Res., 90(A5), 4069–4078, doi:10.1029/JA090iA05p04069, 1985.

Gonzalez, W. D., and Mozer, F. S.: A quantitative model for the potential resulting from reconnection with an arbitrary interplanetary magnetic field, J. Geophys. Res., 79(28), 4186–4194, doi:10.1029/JA079i028p04186, 1974.

Gosling, J. T., Thomsen, M. F., Bame, S. J., Onsager, T. G., and Russell, C. T.: The electron edge of low latitude boundary layer during accelerated flow events, Geophys. Res. Lett., 17, 1833–1836, doi:10.1029/GL017i011p01833, 1990b.

Greenwald, R. A., et al.: DARN/SuperDARN: A global view of the dynamics of high-latitude convection, Space Sci. Rev., 71, 761–796, 1995.

Haerendel, G., Paschmann, G., Sckopke, N., Rosenbauer, H., and Hedgecock, P. C., The frontside boundary layer of the magnetosphere and the problem of reconnection, J. Geophys. Res., 83(A7), 3195–3216, doi:10.1029/JA083iA07p03195, 1978.

Hasegawa, H., et al., Decay of mesoscale flux transfer events during quasi‐continuous spatially extended reconnection at the magnetopause, Geophys. Res. Lett., 43, 4755–4762, doi:10.1002/2016GL069225, 2016.

Haynes, A. L., and Parnell, C. E., A method for finding three-dimensional magnetic skeletons, *Phys. Plasmas*, **17**, 092903, doi:10.1063/1.3467499, 2010.

Huba, J. D., and Rudakov, L. I.: Three-dimensional Hall magnetic reconnection, Phys. Plasmas, 9, 4435, 2002.

Hudson, P. D., Discontinuities in an anisotropic plasma and their identification in the solar wind, Planet. Space Sci., 18, 1611–1622, 1970.

Jain, N., Büchner, J., Dorfman, S., Ji, H., and Sharma, A. S.: Current disruption and its spreading in collisionless magnetic reconnection, Phys. Plasmas 20, 112101, 2013.

Komar, C. M., Cassak, P. A., Dorelli, J. C., Glocer, A., and Kuznetsova, M. M., Tracing magnetic separators and their dependence on IMF clock angle in global magnetospheric simulations, J. Geophys. Res. Space Physics, 118, 4998–5007, doi:10.1002/jgra.50479, 2013.

Kuo, H., Russell, C. T., and Le, G., Statistical studies of flux transfer events, *J. Geophys. Res.*, 100(A3), 3513–3519, doi: 10.1029/94JA02498, 1995.

Laitinen, T. V., Janhunen, P., Pulkkinen, T. I., Palmroth, M., and Koskinen, H. E. J., On the characterization of magnetic reconnection in global MHD simulations, *Ann. Geophys.*, **24**, 3059–3069, 2006.

Laitinen, T. V., Palmroth, M., Pulkkinen, T. I., Janhunen, P., and Koskinen, H. E. J.: Continuous reconnection line and pressure-dependent energy conversion on the magnetopause in a global MHD model, *J. Geophys. Res.*, **112**, A11201, doi:10.1029/2007JA012352, 2007.

Lapenta, G., Krauss-Varban, D., Karimabadi, H., Huba, J. D., Rudakov, L. I., and Ricci, P.: Kinetic simulations of X-line expansion in 3D reconnection, Geophys. Res. Lett., 33, L10102, doi:10.1029/2005GL025124, 2006.

Lee, L. C., and Fu, Z. F., A theory of magnetic flux transfer at the earth's magnetopause, *Geophys. Res. Lett.*, **12**, 105, 1985.

Lockwood, M., Sandholt, P. E., and Cowley, S. W. H.: Dayside auroral activity and momentum transfer from the solar wind, *Geophys. Res. Lett.*, **16**, 33, 1989.

Lockwood, M., and Smith, M. F.: Low altitude signatures of the cusp and flux transfer events, *Geophys. Res. Lett.*, **16**, 879–882, 1989.

Lockwood, M., Cowley, S. W. H., Sandholt, P. E., and Lepping, R. P., The ionospheric signatures of flux transfer events and solar wind dynamic pressure changes, J. Geophys. Res., 95(A10), 17113–17135, doi:10.1029/JA095iA10p17113, 1990.

Lockwood, M., and Smith, M. F., Low and middle altitude cusp particle signatures for general magnetopause reconnection rate variations: 1. Theory, *J. Geophys. Res.*, 99(A5), 8531–8553, doi:10.1029/93JA03399, 1994.

Lockwood, M., et al: Co-ordinated Cluster and ground-based instrument observations of transient changes in the magnetopause boundary layer during an interval of predominantly northward IMF: Relation to reconnection pulses and FTE signatures, *Ann. Geophys.*, **19**, 1613–1640, doi:10.5194/angeo-19-1613-2001, 2001.

Luhmann, J. G., Walker, R. J., Russell, C. T., Crooker, N. U., Spreiter, J. R., and Stahara, S. S.: Patterns of potential magnetic field merging sites on the dayside magnetopause, *J. Geophys. Res.*, **89**, 1739–1742, doi:10.1029/JA089iA03p01739, 1984.

Lui, A. T. Y., and Sibeck, D. G.: Dayside auroral activities and their implications for impulsive entry processes in the dayside magnetosphere, *J. Atmos. Terr. Phys.*, **53**, 219, 1991.

McFadden, J. P., et al., The THEMIS ESA plasma instrument and in-flight calibration, *Space Sci. Rev.*, **141**, 277–302, 2008.

McWilliams, K. A., Yeoman, T. K., and Provan, G.: A statistical survey of dayside pulsed ionospheric flows as seen by the CUTLASS Finland HF radar, Ann. Geophys., 18, 445–453, doi:10.1007/s00585‐000‐0445‐8, 2000.

McWilliams, K. A., Yeoman, T.K., and Cowley, S.W.H.: Two-dimensional electric field measurements in the ionospheric footprint of a flux transfer event, Annales Geophysicae, 18, pp. 1584–1598, 2001a.

McWilliams, K. A., Yeoman, T.K., Sigwarth, J.B., Frank, L.A., and Brittnacher, M.:The dayside ultraviolet aurora and convection responses to a southward turning of the interplanetary magnetic field, Annales Geophysicae, 17, pp. 707–721, 2001b.

McWilliams, K. A., Yeoman, T.K., Sibeck, D.G., Milan, S.E., Sofko, G.J., Nagai, T., Mukai, T., Coleman, I.J., Hori, T., and Rich, F.J., Simultaneous observations of magnetopause flux transfer events and of their associated signatures at ionospheric altitudes, Annales Geophysicae, 22, pp. 2181–2199, 2004.

Milan, S. E., M. Lester, S. W. H. Cowley, and M. Brittnacher (2000), Convection and auroral response to a southward turning of the IMF: Polar UVI, CUTLASS, and IMAGE signatures of transient magnetic flux transfer at the magnetopause, J. Geophys. Res., 105(A7), 15741–15755, doi:10.1029/2000JA900022.

Milan, S. E., Imber, S. M., Carter, J. A., Walach, M.-T., and Hubert, B.: What controls the local time extent of flux transfer events?, J. Geophys. Res. Space Physics, 121, 1391–1401, doi:10.1002/2015JA022012, 2016.

Moen, J., Carlson, H. C., Milan, S. E., Shumilov, N., Lybekk, B., Sandholt, P. E., and Lester, M.: On the collocation between dayside auroral activity and coherent HF radar backscatter, Ann. Geophys., 18, 1531-1549, https://doi.org/10.1007/s00585-001-1531-2, 2000.

Nakamura, T. K. M., Nakamura, R., Alexandrova, A., Kubota, Y., and Nagai, T.: Hall magnetohydrodynamic effects for three-dimensional magnetic reconnection with finite width along the direction of the current, J. Geophys. Res., 117, A03220, doi:10.1029/2011JA017006, 2012.

Neudegg, D. A., Yeoman, T. K., Cowley, S. W. H., Provan, G., Haerendel, G., Baumjohann, W., Auster, U., Fornacon, K.-H., Georgescu, E., and Owen, C. J.: A flux transfer event observed at the magnetopause by the Equator-S spacecraft and in the ionosphere by the CUTLASS HF radar, Ann. Geophysicae, 17, 707, 1999.

Neudegg, D. A., et al., A survey of magnetopause FTEs and associated flow bursts in the polar ionosphere, *Ann. Geophys.*, **18**, 416, 2000.

Nishitani, N., Ogawa, T., Pinnock, M., Freeman, M. P., Dudeney, J. R., Villain, J.-P., Baker, K. B., Sato, N., Yamagishi, H., and Matsumoto, H.: A very large scale flow burst observed by the SuperDARN radars, J. Geophys. Res., 104(A10), 22469–22486, doi:10.1029/1999JA900241, 1999.

Newell, P. T., Meng, C.-I., Sibeck, D. G., and Lepping, R.: Some low-altitude cusp dependencies on the interplanetary magnetic field, J. Geophys. Res., 94(A7), 8921–8927, doi:10.1029/JA094iA07p08921, 1989.

Newell P. T., and Meng C.-I.: Ion acceleration at the equatorward edge of the cusp: Low-altitude observations of patchy merging, Geophys. Res. Lett., 18, 1829–1832, doi:10.1029/91GL02088, 1991.

Newell, P. T., and Meng, C. ‐ I : Ionospheric projections of magnetospheric regions under low and high solar wind conditions, J. Geophys. Res., 99, 273, 1994.

Newell, P. T., Sotirelis, T., Liou, K., Meng, C. ‐ I. and Rich, F. J., A nearly universal solar wind ‐ magnetosphere coupling function inferred from 10 magnetospheric state variables, J. Geophys. Res., 112, A01206, doi: 10.1029/2006JA012015, 2007b.

Tsyganenko, N. A., Modeling the Earth's magnetospheric magnetic field confined within a realistic magnetopause, J. Geophys. Res., 100(A4), 5599–5612, doi:10.1029/94JA03193, 1995.

Oksavik, K., Moen, J. and Carlson, H. C.: High-resolution observations of the small-scale flow pattern associated with a poleward moving auroral form in the cusp, *Geophys. Res. Lett.*, **31**, L11807, doi:10.1029/2004GL019838, 2004.

Oksavik, K., Moen, J., Carlson, H. C., Greenwald, R. A., Milan, S. E., Lester, M., Denig, W. F., and Barnes, R. J.: Multi-instrument mapping of the small-scale flow dynamics related to a cusp auroral transient, *Ann. Geophys.*, **23**, 2657–2670, 2005.

Paschmann, G., et al.: Plasma acceleration at the Earth's magnetopause: Evidence for magnetic reconnection, Nature, 282, 243, 1979.

Paschmann, G., et al.: The magnetopause for large magnetic shear: AMPTE/IRM observations, *J. Geophys. Res.*, **91**, 11,099, 1986.

Petrinec, S. M., and Fuselier, S. A.: On continuous versus discontinuous neutral lines at the dayside magnetopause for southward interplanetary magnetic field, Geophys. Res. Lett., 30(10), 1519, doi:10.1029/2002GL016565, 2003.

Phan, T. D., and Paschmann, G.: Low‐latitude dayside magnetopause and boundary layer for high magnetic shear: 1. Structure and motion, J. Geophys. Res., 101, 7801–7815, doi:10.1029/95JA03752, 1996.

Phan, T.-D., et al.: Extended magnetic reconnection at the Earth's magnetopause from detection of bi-directional jets, *Nature*, **404**, 848, 2000.

Phan, T.D., Freeman, M.P., Kistler, L.M. et al, Evidence for an extended reconnection line at the dayside magnetopause, Earth Planet Sp 53: 619. https://doi.org/10.1186/BF03353281, 2000.

Phan, T., et al.: Simultaneous Cluster and IMAGE observations of cusp reconnection and auroral proton spot for northward IMF, Geophys. Res. Lett., 30(10), 1509, doi:10.1029/2003GL016885, 2003.

Phan, T. D., Hasegawa, H., Fujimoto, M., Oieroset, M., Mukai, T., Lin, R. P., and Paterson, W. R.: Simultaneous Geotail and Wind observations of reconnection at the subsolar and tail flank magnetopause, Geophys. Res. Lett., 33, L09104,doi:10.1029/2006GL025756, 2006.

Phan, T. D., Paschmann, G., Gosling, J. T., Oieroset, M., Fujimoto, M., Drake, J. F., and Angelopoulos, V.: The dependence of magnetic reconnection on plasma $\beta$ and magnetic shear: Evidence from magnetopause observations, Geophys. Res. Lett., 40, 11–16, doi:10.1029/2012GL054528, 2013.

Pinnock, M., Rodger, A. S., Dudeney, J. R., Baker, K. B., Newell, P. T., Greenwald, R. A., and Greenspan, M. E.: Observations of an enhanced convection channel in the cusp ionosphere, J. Geophys. Res., 98, 3767–3776, 1993.

Pinnock, M., Rodger, A. S., Dudeney, J. R., Rich, F., and Baker, K. B.: High spatial and temporal resolution observations of the ionospheric cusps, *Ann. Geophys.*, **13**, 919–925, 1995.

Pinnock, M & Rodger, A., On determining the noon polar cap boundary from SuperDARN HF radar backscatter characteristics. Annales Geophysicae. 18. 10.1007/s00585-001-1523-2, 2001.

Pinnock, M., Chisham, G., Coleman, I. J., Freeman, M. P., Hairston, M., and Villain, J.-P.: The location and rate of dayside reconnection during an interval of southward interplanetary magnetic field, Ann. Geophys., 21, 1467–1482, 2003.

Plaschke F, Hietala H., Angelopoulos V.: Anti-sunward high-speed jets in the subsolar magnetosheath. Ann. Geophys. 2013;31:1877–1889. doi:10.5194/angeo-31-1877-2013, 2013.

Ponomarenko, P. V., Waters, C. L., and Menk, F. W.: Factors determining spectral width of HF echoes from high latitudes, Ann. Geophys., 25, 675-687, https://doi.org/10.5194/angeo-25-675-2007, 2007.

Provan, G. & Yeoman, T.K.: Statistical observations of the MLT, latitude and size of pulsed ionospheric flows with the CUTLASS Finland radar, Annales Geophysicae, 17: 855. https://doi.org/10.1007/s00585-999-0855-1, 1999.

Provan, G., Yeoman, T. K., and Milan, S. E., CUTLASS Finland radar observations of the ionospheric signatures of flux transfer events and the resulting plasma flows, *Ann. Geophys.*, **16**, 1411–1422, 1998.

Ruohoniemi, J. M., Greenwald, R. A., Baker, K. B., Villain, J.-P., Hanuise, C., and Kelly, J.: Mapping high-latitude plasma convection with coherent HF radars, J. Geophys. Res., 94(A10), 13463–13477, doi:10.1029/JA094iA10p13463, 1989.

Ruohoniemi, J. M., and Baker, K. B.: Large-scale imaging of high-latitude convection with Super Dual Auroral Radar Network HF radar observations, J. Geophys. Res., 103(A9), 20797–20811, doi:10.1029/98JA01288, 1998.

Russell, C. T., and Elphic, R. C.: ISEE observations of flux transfer events at the dayside magnetopause, Geophys. Res. Lett., 6(1), 33–36, doi:10.1029/GL006i001p00033, 1979.

Sandholt, P. E., Deehr, C. S., Egeland, A., Lybekk, B., Viereck, R., and Romick, G. J.: Signatures in the dayside aurora of plasma transfer from the magnetosheath, J. Geophys. Res., 91(A9), 10063–10079, doi:10.1029/JA091iA09p10063, 1986.

Sandholt, P. E., Lockwood, M., Oguti, T., Cowley, S. W. H., Freeman, K. S. C., Lybekk, B., Egeland, A., and Willis, D. M.: Midday auroral breakup events and related energy and momentum transfer from the magnetosheath, J. Geophys. Res., 95(A2), 1039–1060, doi:10.1029/JA095iA02p01039, 1990.

Sandholt, P. E., et al.: Cusp/cleft auroral activity in relation to solar wind dynamic pressure, interplanetary magnetic field $B_z$ and $B_y$ , J. Geophys. Res., 99(A9), 17323–17342, doi:10.1029/94JA00679, 1994.

Scholer, M.: Magnetic flux transfer at the magnetopause based on single x line bursty reconnection, *Geophys. Res. Lett.*, **15**, 291, 1988.

Scholer, M., Sidorenko, I., Jaroschek, C. H., Treumann, R. A., and Zeiler, A.: Onset of collisionless magnetic reconnection in thin current sheets: Three-dimensional particle simulations, *Phys. Plasmas*, **10**(9), 3521–3527, 2003.

Shay, M. A., Drake, J. F., Swisdak, M., Dorland, W., and Rogers, B. N.: Inherently three dimensional magnetic reconnection: A mechanism for bursty bulk flows? Geophys. Res. Lett., 30(6), 1345, doi:10.1029/2002GL016267, 2003.

Shepherd, L. S., and Cassak, P. A.: Guide field dependence of 3-D X-line spreading during collisionless magnetic reconnection, J. Geophys. Res., 117, A10101, doi:10.1029/2012JA017867, 2012.

Smith, M., Lockwood, F.M., Cowley, S.W.H.: The statistical cusp: a simple flux transfer event model, *Planet Space Sci.*, 1992

Sonnerup, B. U. Ö., and Cahill Jr., L. J.: Magnetopause structure and attitude from Explorer 12 observations, *J. Geophys. Res.*, **72**, 171, 1967.

Sonnerup, B. U.: Magnetopause reconnection rate, J. Geophys. Res., 79(10), 1546–1549, doi:10.1029/JA079i010p01546, 1974.

Southwood, D. J.: Theoretical aspects of ionosphere ‐ magnetosphere ‐ solar wind coupling, Adv. Space Res., 5(4), 7–14, doi:10.1016/0273 ‐ 1177(85)90110 ‐ 3, 1985.

Southwood, D. J.: The ionospheric signature of flux transfer events, *J. Geophys. Res.*, **92**, 3207, 1987.

Southwood, D. J., Farrugia, C. J., and Saunders, M. A.: What are flux transfer events? *Planet. Space Sci.*, **36**, 503, 1988.

Thorolfsson, A., Cerisier, J.-C., Lockwood, M., Sandholt, P. E., Senior, C. and Lester, M.: Simultaneous optical and radar signatures of poleward-moving auroral forms, *Ann. Geophys.*, **18**, 1054, 2000.

Trattner, K. J., Fuselier, S. A., and Petrinec, S. M.: Location of the reconnection line for northward interplanetary magnetic field, J. Geophys. Res., 109, A03219, doi:10.1029/2003JA009975, 2004.

Trattner, K. J., Mulcock, J. S., Petrinec, S. M., and Fuselier, S. A.: Probing the boundary between antiparallel and component reconnection during southward interplanetary magnetic field conditions, *J. Geophys. Res.*, 112, A08210, doi:10.1029/2007JA012270, 2007.

Trattner, K. J., Fuselier, S. A., Petrinec, S. M., Yeoman, T. K., Escoubet, C. P., and Reme, H.: The reconnection sites of temporal cusp structures, J. Geophys. Res., 113, A07S14, doi:10.1029/2007JA012776, 2008.

Trattner, K. J., Burch, J. L., Ergun, R., Eriksson, S., Fuselier, S. A., Giles, B. L., … Wilder, F. D. :The MMS dayside magnetic reconnection locations during phase 1 and their relation to the predictions of the maximum magnetic shear model. Journal of Geophysical Research: Space Physics, 122, 11,991–12,005. https://doi.org/10.1002/2017JA024488, 2017.

Trenchi, L., Marcucci, M. F., Pallocchia, G., Consolini, G., Bavassano Cattaneo, M. B., Di

Lellis, A. M., Rème, H., Kistler, L., Carr, C. M., and Cao, J. B.: Occurrence of reconnection jets at the dayside magnetopause: Double star observations, J. Geophys. Res., 113, A07S10, doi:10.1029/2007JA012774, 2008.

Tsyganenko, N. A.: A magnetospheric magnetic field model with a warped tail current sheet, Planet. Space Sci., 87, 5, 1989

Tsyganenko, N. A.: Modeling the Earth's magnetospheric magnetic field confined within a realistic magnetopause, J. Geophys. Res., 100(A4), 5599–5612, doi:10.1029/94JA03193, 1995.

Tsyganenko, N. A.: A model of the magnetosphere with a dawn-dusk asymmetry, 1, Mathematical structure, J. Geophys. Res., 107(A8), doi:10.1029/2001JA000219, 2002a.

Tsyganenko, N. A.: A model of the near magnetosphere with a dawn-dusk asymmetry, 2, Parameterization and fitting to observations, J. Geophys. Res., 107(A8), doi:10.1029/2001JA000220, 2002b.

Walsh, B. M., Foster, J. C., Erickson, P. J., and Sibeck, D. G.: Simultaneous ground- and space-based observations of the plasmaspheric plume and reconnection, *Science*, **343**, 1122–1125, doi:10.1126/science.1247212, 2014a.

Walsh, B. M., Phan, T. D., Sibeck, D. G., and Souza, V. M.: The plasmaspheric plume and magnetopause reconnection, Geophys. Res. Lett., 41, 223–228, doi:10.1002/2013GL058802, 2014b.

Walsh, B. M., Komar, C. M., and Pfau-Kempf, Y.: Spacecraft measurements constraining the spatial extent of a magnetopause reconnection X line, Geophys. Res. Lett., 44, 3038–3046, doi:10.1002/2017GL073379, 2017.

Wang, Y., et al.: Initial results of high-latitude magnetopause and low-latitude flank flux transfer events from 3 years of Cluster observations, J. Geophys. Res., 110, A11221, doi:10.1029/2005JA011150, 2005.

Wang, J., et al., TC1 and Cluster observation of an FTE on 4 January 2005: A close conjunction, Geophys. Res. Lett., 34, L03106, doi:10.1029/2006GL028241, 2007.

Wild, J. A., Cowley, S. W. H., Davies, J. A., Khan, H., Lester, M., Milan, S. E., Provan, G., Yeoman, T. K., Balogh, A., Dunlop, M. W., Fornacon, K.-H., and Georgescu, E.: First simultaneous observations of flux transfer events at the high-latitude magnetopause by the Cluster spacecraft and pulsed radar signatures in the conjugate ionosphere by the CUTLASS and EISCAT radars, Ann. Geophys., 19, 1491–1508, 2001.

Wild, J. A., Milan, S. E., Davies, J. A., Cowley, S. W. H., Carr, C. M., and Balogh, A.: Double Star, Cluster, and groundbased observations of magnetic reconnection during an interval of duskward oriented IMF: preliminary results, Ann. Geophys., 23, 2903–2907, 2005.

Wild, J. A., Milan, S. E., Davies, J. A., Dunlop, M. W., Wright, D. M., Carr, C. M., Balogh, A., Reme, H., Fazakerley, A. N., ` and Marchaudon, A.: On the location of dayside magnetic reconnection during an interval of duskward oriented IMF, Ann. Geophys., 25, 219–238, 2007.

Zhang, Q.-H., et al.: Simultaneous tracking of reconnected flux tubes: Cluster and conjugate SuperDARN observations on 1 April 2004, *Ann. Geophys.*, **26**, 1545–1557, doi:10.5194/angeo-26-1545-2008, 2008.

Zou, Y., Walsh, B. M., Nishimura, Y., Angelopoulos, V., Ruohoniemi, J. M., McWilliams, K. A., & Nishitani, N. Spreading speed of magnetopause reconnection X-lines using ground-satellite coordination. Geophysical Research Letters, 45. https://doi.org/10.1002/2017GL075765, 2018.

Figure 1a: OMNI IMF condition on Feb 2, 2013. Figure 1b: THE and THA locations projected to the GSM X-Y plane. The inner curve marks the magnetopause and the outer curve marks the bow shock.

Figure 2a: SuperDARN LOS speeds (color tiles) and merged velocity vectors (color arrows) in the Altitude adjusted corrected geomagnetic (*AACGM*) coordinates. The FOVs of the RKN, INV, and CLY radars are outlined with the black dashed lines. The colors of the tiles indicate the LOS speeds away from the radar. The colors and the lengths of the arrows indicate the merged velocity magnitudes and the arrow directions indicate the velocity directions. Red and anti-sunward directed flows are the ionospheric signature of magnetopause reconnection. The dashed magenta lines mark the flow western and eastern boundaries. The open-closed field line boundary was delineated by the dashed black curve marked by the "OCB" marker. The satellite footprints under the T89 are shown as the THE and THA marker. Figure 2b: Similar to Figure 2a but showing SECS velocity vectors (color arrows). Figure 2c: Similar to Figure 2a but showing SHF velocity vectors (color arrows). Figure 2d: SuperDARN spectral width measurements (color tiles). The red contour marks localized enhanced soft electron precipitation. Figure 2e: Time evolution of the northward component of SECS velocities along 79° MLAT. Figure 2f: Profile of convection velocities along 79° MLAT at 1929 UT as a function of the distance from magnetic noon. The profile in black is based on the LOS measurements and the profile in red is the northward component of the SECS velocities. The FWHM is determined based on each profile. Figures 2g-j: THE measured magnetic field (0.25 s resolution), ion energy flux (3 s), ion density (3 s), and ion velocity (3 s). The ion measurements were taken from ground ESA moments. The magnetic field and the ion velocity components are displayed in the LMN boundary normal coordinate system.

The magnetopause crossing is shaded in pink. Figure 2k: THE ion distribution function on the bulk velocity-magnetic field plane. The small black line indicates the direction and the bulk velocity of the distributions. Figures 2l-p: THA measurements in the same format as in Figures 2g-k. Figures 2q-z: THA and THE measurements during a subsequent magnetopause crossing shown in the same format as in Figures 2g-p.

Figures 3a-c: Snapshots of spectral width measurements around the space-ground conjunction time and longitude. The open-closed field line boundary is drawn as the dashed black line. Figures 3d-f: time series of the spectral width measurements along INV beams 4, 7, and 10, as a function of latitude, from which the motion of the open-closed field line boundary can be derived. Figure 3g: the electric field along the open-closed field line boundary in the frame of boundary (solid) and in the rest frame (dashed) following Pinnock et al. [2003], Freeman et al. [2007], Chisham et al. [2008]. The former is the reconnection electric field.

Figure 4: OMNI IMF condition and THEMIS satellite locations on Apr 19, 2015 in a similar format to Figure 1.

Figure 5. THEMIS and SuperDARN measurements of reconnection bursts on Apr 19, 2015 in a similar format to Figure 2. The velocity time evolution in Figure 5e and the velocity profile in Figure 5f are taken along 78° MLAT.

Figure 6. OMNI IMF condition and THEMIS satellite locations on Apr 29, 2015 in a similar format to Figure 1.

Figure 7. THEMIS and SuperDARN measurements of reconnection bursts on Apr 29, 2015 in a similar format to Figure 2. The velocity time evolution in Figure 7e and the velocity profile in Figure 7f are taken along 79° MLAT. The two branches of the LOS velocity profile in Figure 7f are based on INV and RKN LOS data. The magnetic field and plasma velocities measured by spacecraft are displayed in the GSM coordinates.

Figure 8. Comparison of the IMF and solar wind driving conditions between the reconnection events on Feb 2, 2013, Apr 19, 2015, and Apr 29, 2015. From top to bottom: IMF in GSM coordinates, IMF clock angle, solar wind speed, and solar wind dynamic pressure. The red vertical lines mark the times of the satellite-ground conjunction.

Figure 1.

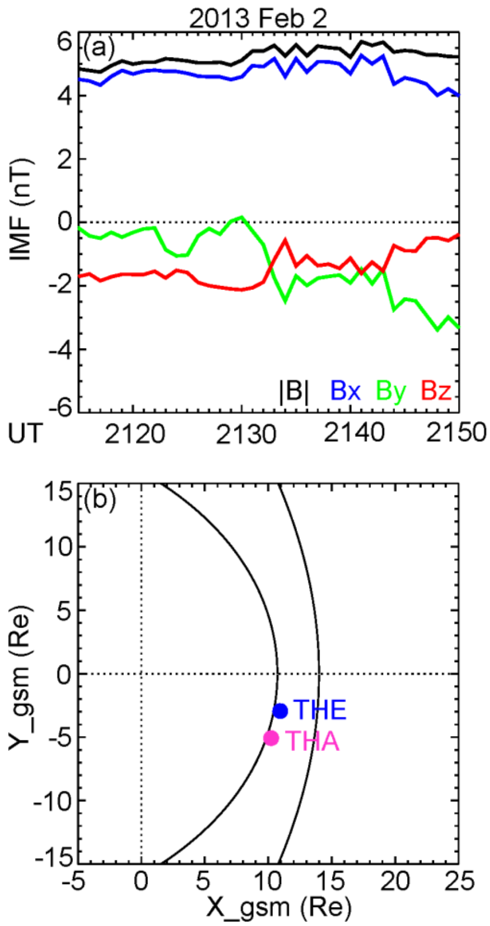
2013 Feb 2
(a)
IMF (nT)
|B| Bx By Bz
UT
2120
2130
2140
2150
(b)
Y_gsm (Re)
X_gsm (Re)
THE
THA

Figure 2.

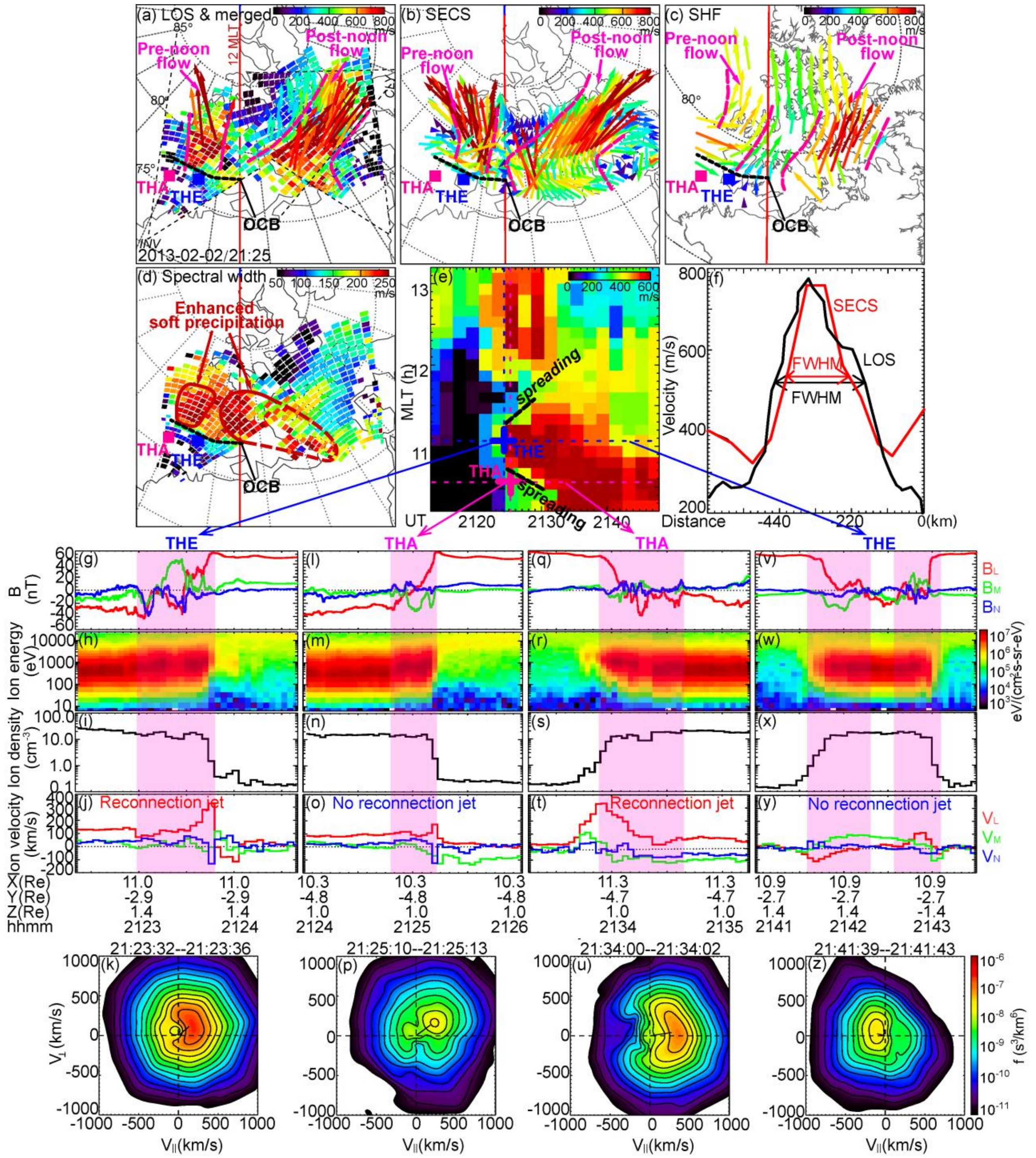
(a) LOS & merged
(b) SECS
(c) SHF
Pre-noon flow
Post-noon flow
12 MLT
THA
THE
OCB
2013-02-02/21:25
(d) Spectral width
Enhanced soft precipitation
(e)
spreading
MLT (h)
UT
(f)
SECS
LOS
FWHM
Velocity (m/s)
Distance
B (nT)
Ion energy (eV)
Ion density (cm⁻³)
Ion velocity (km/s)
Reconnection jet
No reconnection jet
X(Re)
Y(Re)
Z(Re)
hhmm
21:23:32--21:23:36
21:25:10--21:25:13
21:34:00--21:34:02
21:41:39--21:41:43
V⊥(km/s)
V||(km/s)

Figure 3.

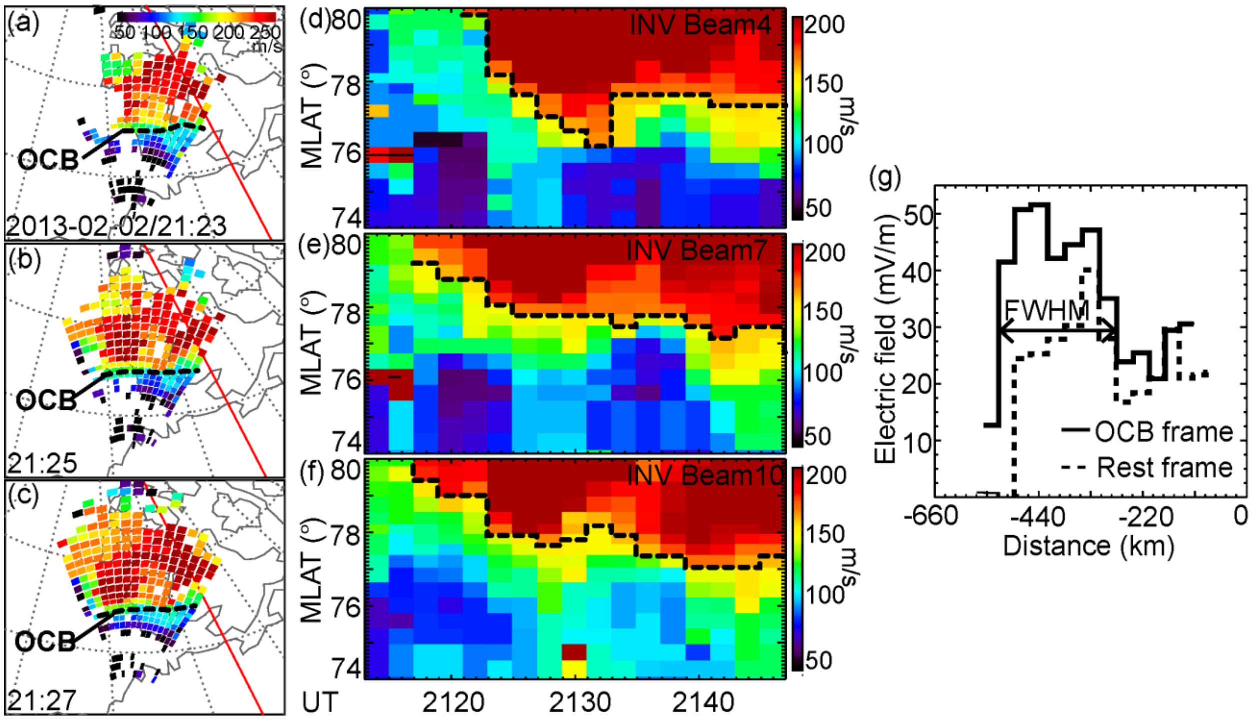
(a)
50 100 150 200 250
m/s
OCB
2013-02-02/21:23
(b)
OCB
21:25
(c)
OCB
21:27
(d)
INV Beam4
(e)
INV Beam7
(f)
INV Beam10
MLAT (°)
80
78
76
74
200
150
100
50
m/s
UT
2120
2130
2140
(g)
Electric field (mV/m)
50
40
30
20
10
FWHM
OCB frame
Rest frame
-660
-440
-220
0
Distance (km)

Figure 4.

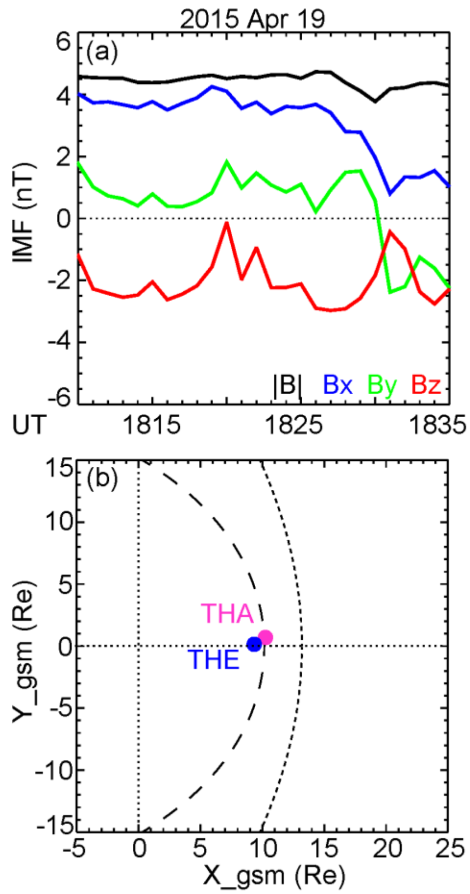
2015 Apr 19
(a)
IMF (nT)
|B| Bx By Bz
UT
1815
1825
1835
(b)
THA
THE
Y_gsm (Re)
X_gsm (Re)

Figure 5.

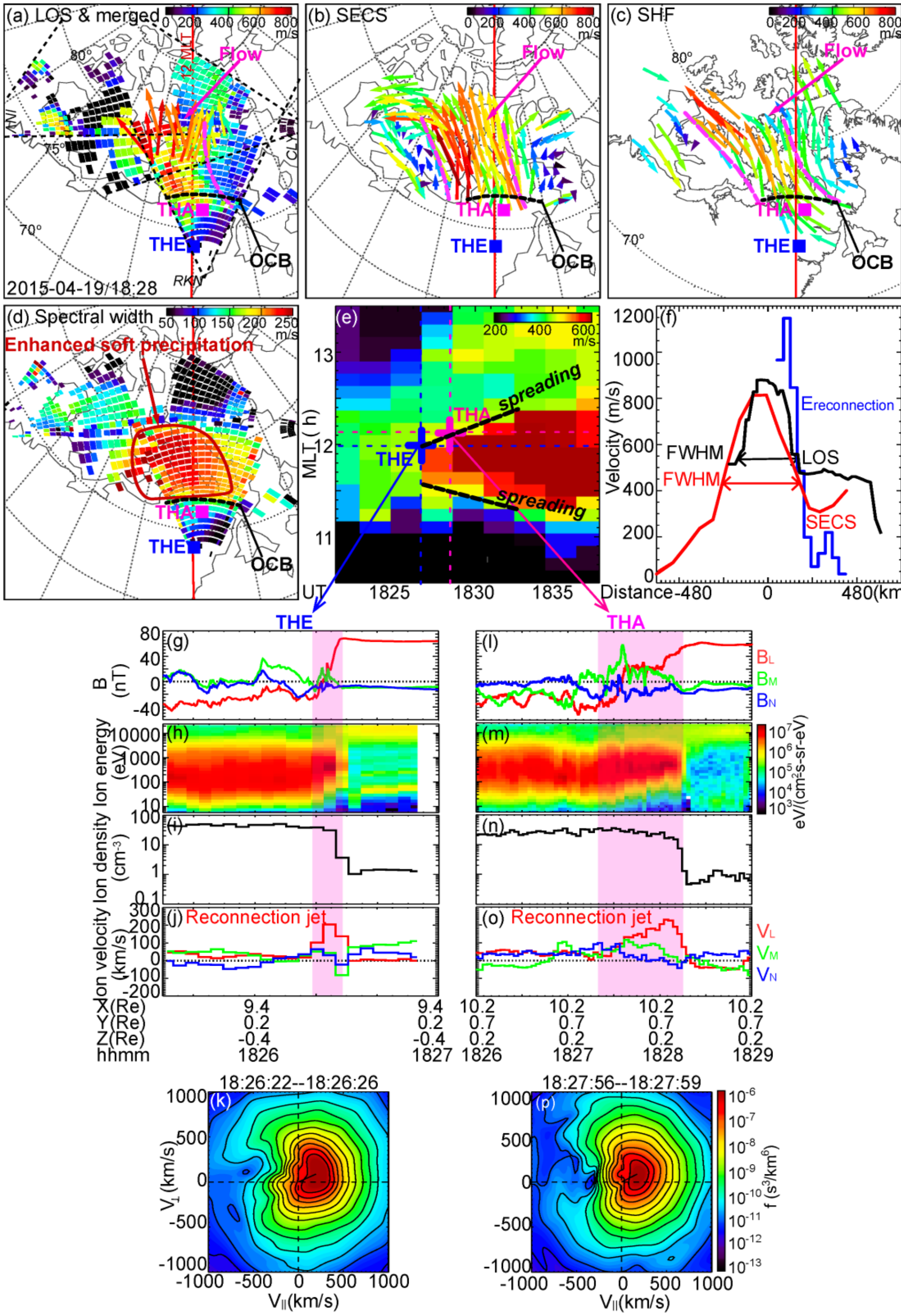

(a) LOS & merged
(b) SECS
(c) SHF
(d) Spectral width
(e)
(f)
Flow
THA
THE
OCB
2015-04-19/18:28
Enhanced soft precipitation
spreading
MLT (h)
UT
Velocity (m/s)
Electric field (mV/m)
Ereconnection
FWHM
LOS
SECS
Distance
(km)
(g)
(h)
(i)
(j) Reconnection jet
(k)
(l)
(m)
(n)
(o) Reconnection jet
(p)
B (nT)
Ion energy (eV)
Ion density (cm-3)
Ion velocity (km/s)
BL
BM
BN
VL
VM
VN
eV/(cm2-s-sr-eV)
X(Re)
Y(Re)
Z(Re)
hhmm
18:26:22--18:26:26
18:27:56--18:27:59
V⊥(km/s)
V||(km/s)
f (s3/km6)

Figure 6.

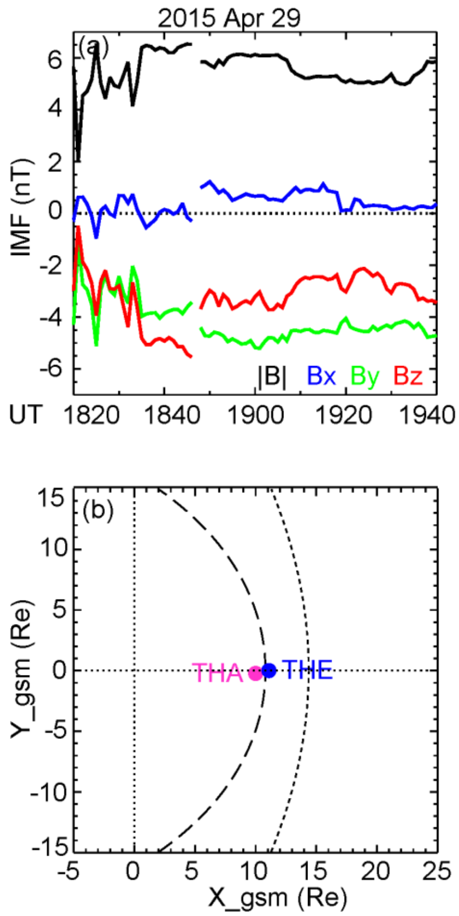
2015 Apr 29
(a)
IMF (nT)
|B| Bx By Bz
UT 1820 1840 1900 1920 1940
(b)
THA
THE
Y_gsm (Re)
X_gsm (Re)

Figure 7.

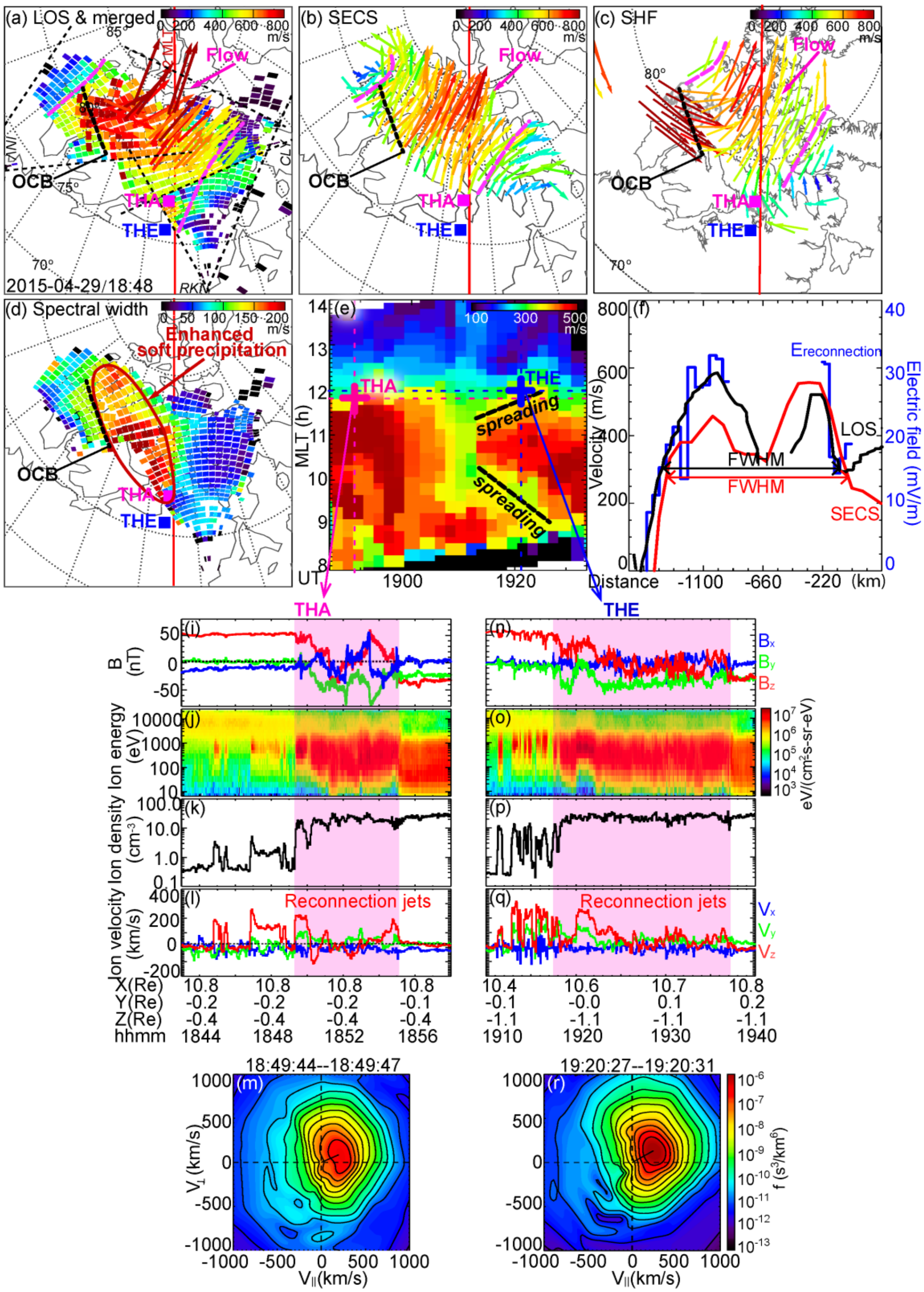

(a) LOS & merged
(b) SECS
(c) SHF
Flow
OCB
THA
THE
2015-04-29/18:48
(d) Spectral width
Enhanced soft precipitation
(e)
MLT (h)
spreading
UT
(f)
Ereconnection
Electric field (mV/m)
Velocity (m/s)
LOS
FWHM
SECS
Distance
(km)
(i)
(j)
(k)
(l)
Reconnection jets
(n)
(o)
(p)
(q)
B (nT)
Ion energy (eV)
Ion density (cm-3)
Ion velocity (km/s)
eV/(cm2-s-sr-eV)
X(Re)
Y(Re)
Z(Re)
hhmm
18:49:44--18:49:47
19:20:27--19:20:31
(m)
(r)
f (s3/km6)


55

Figure 8.

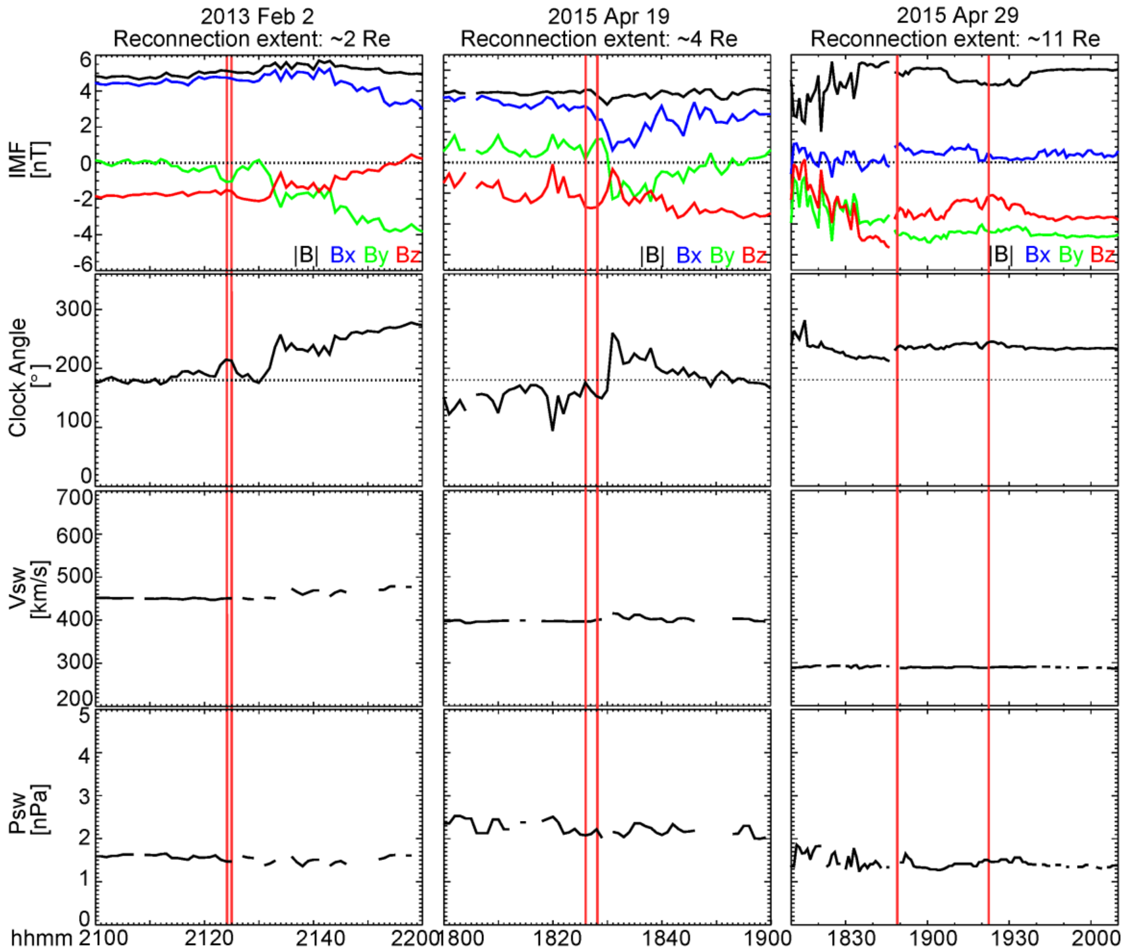
2013 Feb 2
Reconnection extent: ~2 Re
2015 Apr 19
Reconnection extent: ~4 Re
2015 Apr 29
Reconnection extent: ~11 Re
IMF [nT]
|B| Bx By Bz
Clock Angle [°]
Vsw [km/s]
Psw [nPa]
hhmm
2100
2120
2140
2200
1800
1820
1840
1900
1830
1900
1930
2000